JOURNAL OF GUIDANCE, CONTROL, AND DYNAMICS
Vol. 38, No. 9, September 2015

New Solutions for the Perturbed Lambert Problem Using Regularization and Picard Iteration

Robyn M. Woollands*
Texas A&M University, College Station, Texas 77843-3141
Ahmad Bani Younes†
Khalifa University of Science, Technology and Research, Abu Dhabi, United Arab Emirates
and
John L. Junkins‡
Texas A&M University, College Station, Texas 77843-3141

DOI: 10.2514/1.G001028

A new approach for solving two-point boundary value problems and initial value problems using the Kustaanheimo–Stiefel transformation and Modified Chebyshev–Picard iteration is presented. The first contribution is the development of an analytical solution to the elliptic Keplerian Lambert problem based on Kustaanheimo–Stiefel regularization. This transforms the nonlinear three-dimensional orbit equations of motion into four linear oscillators. The second contribution solves the elliptic Keplerian two-point boundary value problem and initial value problem using the Kustaanheimo–Stiefel transformation and Picard iteration. The Picard sequence of trajectories represents a contraction mapping that converges to a unique solution over a finite domain. Solving the Keplerian two-point boundary value problem in Kustaanheimo–Stiefel variables increases the Picard domain of convergence from about one-third of an orbit (Cartesian variables) to over 95% of an orbit (Kustaanheimo–Stiefel variables). These increases in the domain of Picard iteration convergence are independent of eccentricity. The third contribution solves the general spherical harmonic gravity perturbed elliptic two-point boundary value problem using the Kustaanheimo–Stiefel transformation and Picard iteration, and it does not require a Newton-like shooting method for fractional orbit transfers. For multiple revolution transfers, however, a shooting method can make use of the Modified Chebyshev–Picard iteration/Kustaanheimo–Stiefel/initial value problem and the Method of Particular Solutions to obtain solutions given a Keplerian Lambert solution as the starting iterative. The Kustaanheimo–Stiefel perturbed solution is illustrated using a (40,40) degree and order spherical harmonic gravity model. A general three-dimensional recipe is introduced for solving the perturbed Lambert Problem via Modified Chebyshev–Picard iteration without a Newton-like shooting method for the fractional orbit case. The increase in the domain of convergence of the Kustaanheimo–Stiefel transformed, perturbed Lambert problem via Modified Chebyshev–Picard iteration versus the Cartesian Modified Chebyshev–Picard iteration Lambert solution is analogous to the results for the Keplerian case. The three-dimensional two-impulse perturbed Lambert problem is efficiently convergent up to about 85% of the Keplerian orbit period with a (40,40) spherical harmonic gravity model. The efficiency of the current two-point boundary value problem solver is compared with MATLAB's *fsolve*, where Runge–Kutta–Nystrom 12(10) and Gauss–Jackson are the integrators.

I. Introduction

LAMBERT'S problem is the classical two-point boundary value problem (TPBVP) in celestial mechanics, that was first posed and solved by Johann Heinrich Lambert in 1761 [1]. It is known to have a unique solution for the fractional orbit transfer between prescribed positions in a prescribed "time of flight." Solving the problem requires determining the orbital arc (typically, solving for the initial velocity) connecting a prescribed initial position and final position, which correspond to the specified flight time. In the modern literature, Richard Battin [1] developed an immortal, as well as the most widely used, and general algorithm for solving the unperturbed Lambert's problem (Keplerian motion). His algorithm generates not only the unique solution for the fractional orbit case but also the multiple solutions associated with multiple revolution orbit transfers.

The most common solution approach for generalizing the Lambert problem to include perturbations is to use the state transition matrix sensitivity of the final state with respect to the initial velocity and iterate via Newton's method on the three components of initial velocity to "hit" the final desired position at the prescribed final time. The unperturbed Lambert solution [e.g., Battin's Lambert algorithm [1], the *p*-iteration method [2], or the alternative Kustaanheimo–Stiefel (KS) Keplerian Lambert solution presented herein] can be used as a "warm start" to solve the perturbed problem.

One motivation for this research is to respond to the various challenges in space situational awareness (SSA) with a difficult "data association" problem. Short tracks of many newly observed objects, widely separated in time, must be processed to determine orbits and correlate the observations of tracked objects, if possible, with each other and with existing space object databases.

In the current state of the practice, hundreds of thousands of hypotheses must frequently be tested to find feasible preliminary orbits connecting time-displaced short tracks of unknown space objects. These preliminary orbits and the underlying data associations are taken as the starting estimates for further correlation. "Short" tracks may be separated by up to several orbits, so ignoring the effects of perturbations will typically introduce residual errors much larger than the measurement errors, which can corrupt the data association process. In the current state of practice, data association hypotheses are tested for preliminary orbit estimation using the Keplerian Lambert solutions for sufficiently short arcs, but higher precision is needed to accommodate hypothesis testing over longer time intervals. When more than several hundred thousand hypotheses are tested daily (including perturbations), the computational cost can

Presented as Paper 2014-017 at the AAS Guidance, Navigation, and Control Conference, Breckinridge, CO, 31 January–5 February 2014; received 2 September 2014; revision received 6 August 2015; accepted for publication 7 August 2015; published online 9 September 2015.

*Graduate Research Assistant, Department of Aerospace Engineering, TAMU 3141.

†Assistant Professor, Aerospace Engineering Department; ahmad.younes@kustar.ac.ae.

‡Distinguished Professor, Department of Aerospace Engineering, TAMU 3141. Honorary Fellow AIAA.

exceed many CPU days per month. The anticipation of a new space fence giving an order of magnitude increase to 200,000 more presently untrackable debris objects (visible to our sensors) means that already high computational costs are about to dramatically increase. Millions of hypotheses will require testing to solve the data association problems. Also, the "all-on-all" conjunction analysis and probability of collisions will be extremely difficult using existing orbit propagation tools. Thus, the issue of finding an optimal solution to a generally perturbed TPBVP lies near the heart of computational challenges in SSA. The inclusion of perturbations in Lambert's problem and the development of more efficient and robust methods are therefore of strong interest.

II. Chebyshev–Picard Numerical Integration

The preferred numerical integrator used in this paper is known as Modified Chebyshev–Picard iteration (MCPI), although, to help calibrate the results, we use several state-of-the-practice differential equation solvers. MCPI is an attractive numerical method for solving linear or nonlinear differential and integral equations, and a slight modification of the MCPI initial value solver makes the algorithm applicable to TPBVPs. MCPI combines the discoveries of two great mathematicians: Emile Picard (Picard iteration) and Rafnuty Chebyshev (Chebyshev polynomials). MCPI differs from the well-known integrators such as Gauss–Jackson and Runge–Kutta–Nystrom, in that it is an iterative path approximation numerical integrator rather than a time-step extrapolation integrator. That is, a relatively long state trajectory arc is approximated continuously and can be updated at all time nodes simultaneously on each path iteration. As will be evident in the following, the solution of TPBVPs using MCPI does not require a local-linearization-based shooting method. Furthermore, the MCPI approach inherits the important theoretical advantage of the Picard iteration, namely, that over a large domain of time intervals and starting approximations, Picard iteration is a contraction mapping that converges to the solution satisfying both the differential equation and the boundary conditions.

Picard observed that any first-order differential equation [3,4]

$$\frac{\mathrm{d}\boldsymbol{x}(t)}{\mathrm{d}t} = \boldsymbol{f}(t, \boldsymbol{x}(t)), \qquad t \in [t_0, t_f] \tag{1}$$

with an initial condition $\boldsymbol{x}(t_0) = \boldsymbol{x}_0$ can be rearranged, without approximation, to obtain the following integral equation:

$$\boldsymbol{x}(t) = \boldsymbol{x}(t_0) + \int_{t_0}^{t} \boldsymbol{f}(\tau, \boldsymbol{x}(\tau))\,\mathrm{d}\tau \tag{2}$$

This rearrangement does not appear to have made any progress, since the unknown trajectory $\boldsymbol{x}(t)$ is contained within the integrand on the right-hand side. However, given some starting estimate $\boldsymbol{x}^0(t)$ for the path, a sequence of approximate solutions $\boldsymbol{x}^i(t)$, $(i = 1, 2, 3, \ldots, \infty)$ of the true solution $\boldsymbol{x}(t)$ that satisfies this differential equation and the prescribed boundary conditions may be obtained through the Picard iteration using the following Picard sequence of approximate paths $\{\boldsymbol{x}^0(t), \boldsymbol{x}^1(t), \ldots, \boldsymbol{x}^{i-1}(t), \boldsymbol{x}^i(t), \ldots\}$:

$$\boldsymbol{x}^i(t) = \boldsymbol{x}(t_0) + \int_{t_0}^{t} \boldsymbol{f}(\tau, \boldsymbol{x}^{i-1}(\tau))\,\mathrm{d}\tau, \qquad i = 1, 2, \ldots \tag{3}$$

Picard proved an important convergence theorem that essentially states that, for smooth, differentiable single-valued nonlinear functions $\boldsymbol{f}(t, x(t))$, the Picard sequence of trajectories represents a contraction operator that converges to the unique solution of the initial value problem (IVP). That is, there is a time interval $|t_f - t_0| < \delta$ and a starting trajectory $\boldsymbol{x}^0(t)$ satisfying $\|\boldsymbol{x}^0(t) - \boldsymbol{x}(t)\| < \Delta$, for suitable finite bounds (δ, Δ); then, the Picard sequence converges. Bai [3] discussed the literature on estimating the theoretical convergence bounds (δ, Δ). As a practical matter, the available bounds are known to be typically very conservative and, for general nonlinear systems, the convergence domain must be inferred through adaptive numerical methods.

In a first step toward the MCPI method, a finite set of orthogonal Chebyshev polynomials are used as basis functions to approximate the integrand in Eq. (3) along the previous approximate trajectory $\boldsymbol{x}^{i-1}(t)$. Chebyshev polynomials are defined over the domain $\{-1 \le \tau \le 1\}$ and can be generated from the two-term recursion as

$$T_0(\tau) = 1, \qquad T_1(\tau) = \tau,$$
$$T_{k+1}(\tau) = 2\tau T_k(\tau) - T_{k-1}(\tau); \qquad k > 1 \tag{4}$$

Under usually satisfied and known theoretical circumstances, we can show [5] that the Picard sequence is a contraction mapping guaranteed to converge to the solution of Eq. (1) over large time intervals. By daisy chaining in a piecewise continuous fashion, the converged solutions for each successive time segment permit reliably convergent solutions over arbitrary large time intervals. The system dynamics are normalized such that the time span of integration is linearly projected onto the domain $\{-1 \le \tau \le 1\}$ of the Chebyshev polynomials. The orthogonal nature of the basis functions means that the coefficients that linearly combine the basis functions can be computed independently as simple ratios of inner products with no matrix inversion. Thus, $\boldsymbol{f}(t, \boldsymbol{x}(t))$ can be interpolated as a function of time along the previous best approximate trajectory $\boldsymbol{x}^{(i-1)}(t)$. Here, $\boldsymbol{f}(t, \boldsymbol{x}(t))$ is approximated to high precision by

$$\boldsymbol{f}(\tau, \boldsymbol{x}(\tau)) = \sum_{k=0}^{k=N-2}{}' \boldsymbol{F}_k T_k(\tau) \tag{5}$$

For large N, Chebyshev polynomials approach a complete set and, due to orthogonality, no matrix inversions are required to compute the $\boldsymbol{F}_k$ for essentially arbitrary N (although experience indicates that efficiency considerations will encourage us to limit the time segments such that $N < 100$). Thus, we can typically approach machine precision (if desired) for local approximation of the integrand in Eq. (3) on each iteration, and the resulting converged trajectory can approach a machine-precision solution of the differential equation. Since integration is known to be a smoothing operation, if an algebraically exact integral is computed, precision of integrand approximation will not be lost when the integral of Eq. (3) is taken. We took some notational liberties in Eq. (5): we replaced $\boldsymbol{f}(t, \boldsymbol{x}(t))$ by $\boldsymbol{f}(\tau, \boldsymbol{x}(\tau))$ when, in reality $\boldsymbol{f}(\tau, \boldsymbol{x}(\tau))$ is a new function $\boldsymbol{g}(\tau, \boldsymbol{x}(\tau))$ equal to $\boldsymbol{f}(t, \boldsymbol{x}(t))$ multiplied by $(t_f - t_0)/2$, with t replaced by

$$t = t_0 + (1 + \tau)\frac{(t_f - t_0)}{2}$$

For the Keplerian IVP and low to moderate eccentricity, the maximum time interval for convergence of the Picard iteration is just over three orbits [6] and for the Keplerian TPBVP this is about one-third of the period of low to moderate eccentricity orbits [4].

Of course, for daisy chaining of many finite segments, even machine-precision solutions over local segments will eventually accumulate error, and like any method for solving differential equations, these local errors will ultimately degrade the long-term stability and accuracy; the stability and accuracy are complicated functions of the particular differential equations being solved. However, we mention that the long-term stability of Gauss–Jackson 8 (GJ8), RK(12) 10, and the MCPI initial value solver were studied rigorously [7–10] for a family of benchmark problems from orbital mechanics. The results show the MCPI initial value solver to be competitive with both the GJ8 and RK(12)10 differential equation solvers as regards long-term orbit computation accuracy and stability. All three methods were shown capable of preserving over eight-digit accuracy for 30 orbits over a range of low Earth orbit (LEO), medium Earth orbit (MEO), geostationary transfer orbit (GTO), and high Earth orbit (HEO), with the force model including higher-order gravity perturbations.

We mention the distinction between precisely solving the differential equations for a given force model and the physical accuracy of the force model itself. For the current state of knowledge of the gravity field and the upper atmosphere, claiming a physical acceleration accuracy better that 1×10^{-7} m/s^{-2} over one low Earth orbit (LEO) is considered to be beyond the state of the art. This

corresponds to errors in the eighth digit in the ephemeris (position errors of a fraction of a meter). However, the stability of long-term integration and other theoretical convergence considerations dictates that we frequently pursue more accurate solutions for a given force model than the number of digits that corresponds to the physical accuracy of the force model.

Notice that the acceleration approximation is expressed as a linear combination of the Chebyshev basis functions

$$\boldsymbol{f}(\tau, x(\tau)) = \sum_{k=0}^{k=N-2} \boldsymbol{F}_k T_k(\tau)$$

Since τ only appears in the argument of the basis functions, and because integrals of the Chebyshev polynomials project back onto the Chebyshev polynomial basis functions, the approximations for position and velocity are likewise obtained as a linear combination of the basis functions. Integrating the series term by term yields

$$\frac{\mathrm{d}\boldsymbol{x}}{\mathrm{d}\tau} = \sum_{k=0}^{k=N-1}{}' \beta_k T_k(\tau) \equiv \frac{1}{2}\beta_0 T_0(\tau) + \ldots + \beta_k T_k(\tau) + \ldots + \beta_{N-1} T_{N-1}(\tau) \tag{6}$$

and

$$\boldsymbol{x}(\tau) = \sum_{k=0}^{k=N}{}'' \alpha_k T_k(\tau) \equiv \frac{1}{2}\alpha_0 T_0(\tau) + \ldots + \alpha_k T_k(\tau) + \ldots + \frac{1}{2}\alpha_N T_N(\tau) \tag{7}$$

In Eqs. (6) and (7), the Clenshaw [5] Σ', Σ'' notation for inner products is adopted. An obvious, but simultaneously subtle truth is important in Eqs. (3–7). The constants of integration are linearly contained as undetermined coefficients in α_0, α_1, and β_0 that can be determined to rigorously satisfy the boundary conditions. It turns out that there are exactly the required number ($2n$ for a system of n second-order differential equations, n for a system of n first-order differential equations) of free constants to specify any combination of initial position and velocity or terminal position and velocity as boundary conditions. As a consequence, any combination of initial and terminal linear boundary conditions can be imposed exactly on each Picard iteration. So, the distinction between solving an IVP and a TPBVP reduces to how the first one or two linearly contained coefficient vectors in the Chebyshev series are determined as a function of boundary conditions. This truth enables TPBVPs to be solved without a shooting method based on local linearizations with respect to initial conditions. This is accomplished for TPBVPs using a close cousin of the same Picard algorithm used to solve IVPs. Picard iterations converge analogously to refine path approximations, whether solving an IVP or a TPBVP. However, as reported in [3] and consistent with our results in the following, the details of how the boundary constants enter the Picard formulation do affect the time interval over which the Picard sequence converges. The IVP version of Picard iteration typically has about a one order of magnitude larger maximum time interval for convergence than that for the corresponding TPBVP.

As a consequence of the independence and orthogonality of the basis functions, the coefficients multiplying the Chebyshev basis functions may be computed in parallel by independent threads. This is the first of two available layers of parallelization in the MCPI method. The second layer of parallelization is much more important and is enabled by the fact that acceleration at the nodes over a large segment state trajectory $\boldsymbol{x}^{i-1}(t)$ may be computed independently and simultaneously. The integrand function must be computed as a function of the system states along the current approximate trajectory, at the nodes, as required for the discrete inner products leading to the approximation coefficients. These computations can be performed at all nodes simultaneously and fully independently in parallel processor threads. For complicated force models, the parallel computation of the force vectors at N nodes means that the theoretical $(1/N)$ speedup can be approached, since it is obviously easy to avoid using shared memory for independent computations.

A key feature of MCPI is a nonuniform cosine sampling of the $\{-1 \le \tau \le 1\}$ domain of the so-called Chebyshev–Gauss–Lobatto nodes:

$$\tau_j = -\cos\left(\frac{j\pi}{N}\right), \qquad j = 0, 1, 2, \ldots, N \tag{8}$$

This set of samples has higher nodal density near the ± 1 domain boundaries that compensate and approximately minimize the Runge phenomena. This is a common concern whereby larger oscillatory approximation errors may occur near the edges of the domain due to lack of support for the approximation outside the domain. The coefficients that linearly combine the Chebyshev basis functions are approximated by the method of least squares. This generally requires a matrix inversion. However, a consistent choice of basis functions, weights, and node locations to ensure orthogonality means that the matrix required to be inverted in the normal equations of least squares is diagonal. Thus, the inverse is trivial and each of the coefficient vectors corresponding to $T_k(\tau)$ is independent of the computation of all other coefficient vectors. A flow diagram outlining the MCPI methodology is presented in Fig. 1.

The original fusion of orthogonal approximation theory and the Picard iteration was introduced by Clenshaw and Norton in 1963 [5]. Feagin also contributed in this area in 1973, with his doctoral dissertation on Picard iteration using Chebyshev approximation establishing the first vector-matrix version of Picard iteration using orthogonal basis functions [11]. In 1980, Shaver wrote a related dissertation, giving insights on parallel computation using Picard iteration and Chebyshev approximation [12]. Fukushima [13] addressed parallelization of the Picard iteration in a particular computer architecture. His results showed that a particular parallel implementation of his algorithm did not give the theoretical speedup he anticipated.

Bai and Junkins revisited this approach and developed improved algorithms for solving IVPs and TPBVPs [6,4]. They established new convergence insights and optimized the solution of IVPs using vector-matrix formulations that were published in Bai's doctoral dissertation [3]. Bai and Junkins [6,4] also showed that MCPI, when applied to the state/costate differential equations derived from Pontryagin's principle, led to an accurate and efficient means for indirect calculus of variations-based trajectory optimization. The main drawback is the relatively small interval over which the TPBVP associated with the frequently stiff state/costate differential equations are solvable using Picard iteration. This MCPI optimal control algorithm was compared to a pseudospectral solution of example problems and showed improved accuracy, efficiency, and robustness of convergence. These results used Cartesian coordinates; other coordinates and associated differential equations required further investigation. Following this work, Junkins et al. [14–16] and Bani Younes [17] developed methods to include high-order gravity perturbations in order to more accurately represent the motion of satellites orbiting in the vicinity of the Earth.

Since then, enhancements have been made by several investigators. Recent work includes a MATLAB MCPI library [18], variable fidelity and radially adaptive gravity approximations [7,19,20], segmentation/order tuning [21], multiorbit accuracy and numerical stability studies [8], Kustaanheimo–Stiefel regularization [22], and using the method of particular solutions [23] to solve TPBVP [24] and control problems [25]. These studies also included significant benchmarks versus traditional high-order integrators such as Runge–Kutta–Nystrom 12 (10) [RKN(12)10] and Gauss–Jackson eighth order (the most important state-of-the-practice algorithm in orbit mechanics).

It is important to make the distinction between the present implementation of the Picard–Chebyshev algorithms and other related recent attempts to fuse orthogonal approximation and the Picard iteration that claim poor performance statistics compared with various other numerical integrators [26]. The algorithm used in the present study incorporates insights from [7,8,20] that collectively separate it from the independently programmed "MCPI" algorithms used in [26]. One of the key speedups is achieved through local force approximation that takes advantage of the fixed-point nature of the Picard iteration; the approximation nodes quickly converge to the

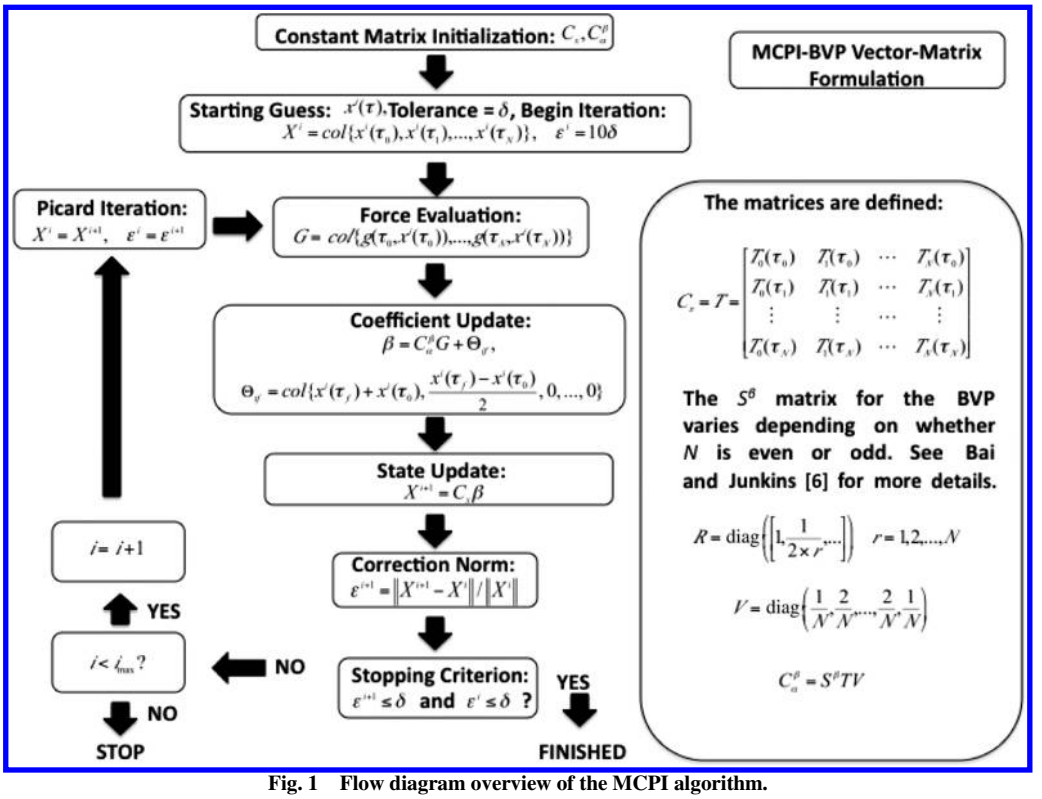

Fig. 1 Flow diagram overview of the MCPI algorithm.

close neighborhood of fixed points in the force field. Most fundamentally, some care is required for integration methods (including MCPI) that have two or more parameters that control efficiency, accuracy, and stability. For example, simply holding fixed the time interval for path approximation as one orbit period will lead to badly suboptimal results. The algorithms in [7,19,21] address the proper tuning and demonstrate a high degree of stability, precision, and efficiency as compared to state-of-the-practice algorithms.

The MCPI method is a fixed-point algorithm; thus, every nodal point converges to a fixed point in the force field. The terminal iterations are in the very near vicinity of a fixed point and following the work of Bani Younes [17], we know local gravity can be accurately approximated with very inexpensive algorithms. As a consequence of the local force approximations, variable fidelity gravity models can be introduced that are several orders of magnitude less expensive than brute force recomputation of the globally valid spherical harmonic series on subsequent neighboring Picard iterations. Other innovations include warm and hot starts computed using Battin's analytical two-body solution [1], radial gravity adaptation [19], and optimal segmentation [21].

Figure 1 applies to a specific finite time segment, which is typically a large fraction of one orbit. The multisegment solutions are straightforward, and the end state of the mth segment becomes the initial state for the $(m+1)$th segment. Tuning for segment lengths and approximation order is addressed in [27].

III. KS Regularization Transformation

Our interest in the KS regularized Lambert's problem is motivated by the results in two classical papers [28,29]. Kriz [29] considered the Keplerian unperturbed problem, and Engels and Junkins [28] developed an approximate solution of the J2-perturbed Lambert problem in KS variables. The present developments go further, considering general perturbations and novel algorithms for efficiently computing the numerical solutions of generally perturbed Lambert problems in KS variables.

The Kustaanheimo–Stiefel transformation [30] is a method for rigorously linearizing, without local approximation, the two-body problem through a judicious coordinate transformation.

We begin by writing the classical differential equations of orbital motion in the most familiar rectangular Cartesian coordinates:

$$\frac{\mathrm{d}^2\boldsymbol{r}}{\mathrm{d}t^2} = -\frac{\mu}{r^3}\boldsymbol{r} + \boldsymbol{F} \tag{9}$$

where $\boldsymbol{r} = [X \quad Y \quad Z \quad 0]^T$, $r = |\boldsymbol{r}|$. The KS transformation involves transforming both the position coordinates and the independent time variable. The position transformation can be written compactly in matrix form as

$$\boldsymbol{r} = \begin{Bmatrix} X \\ Y \\ Z \\ 0 \end{Bmatrix} = L(\boldsymbol{u})\boldsymbol{u},$$
$$\text{where } L(\boldsymbol{u}) = \begin{bmatrix} u_1 & -u_2 & -u_3 & -u_4 \\ u_2 & u_1 & -u_4 & -u_3 \\ u_3 & u_4 & u_1 & u_2 \\ u_4 & -u_3 & u_2 & -u_1 \end{bmatrix}, \quad \boldsymbol{u} = \begin{Bmatrix} u_1 \\ u_2 \\ u_3 \\ u_4 \end{Bmatrix} \tag{10}$$

The most frequently used inverse [22,28,29] transformation is given by

$$\boldsymbol{u} = \begin{Bmatrix} \left(\frac{(r+x)}{2}\right)^{1/2} \\ \frac{y}{(2(r+x))^{1/2}} \\ \frac{z}{\left(2(r+x)\right)^{1/2}} \\ 0 \end{Bmatrix} \tag{11}$$

The operator $L(\boldsymbol{u})$ has many interesting properties [22,28,30], including

$$L^{-1}(\boldsymbol{u}) = \frac{1}{r}L^T(\boldsymbol{u}), \quad \text{and} \quad L(\boldsymbol{u})\boldsymbol{v} = L(\boldsymbol{v})\boldsymbol{u} \tag{12}$$

It is important to note that the second part of Eq. (12) is only valid for the planar case for arbitrary $\boldsymbol{u}$ and $\boldsymbol{v}$. Given a 4-D $\boldsymbol{u}$ vector, $L(\boldsymbol{u})\boldsymbol{v} = L(\boldsymbol{v})\boldsymbol{u}$ holds only if $\boldsymbol{v}$ satisfies $L_4(\boldsymbol{u})\boldsymbol{v} = 0$, i.e., $\boldsymbol{v}$ is perpendicular to the fourth row of $L(\boldsymbol{u})$. This gives rise to [31] the

bilinear constraint ($\phi = L_4(\boldsymbol{u})\boldsymbol{u}' = 0$, and $\phi = 0$ can be verified to be an exact integral of the KS equations of motion developed in the following. For the motion to be physically plausible, the bilinear constraint must be satisfied. This means that the velocity $\boldsymbol{u}'$ in KS variables is at all times orthogonal to $L_4(\boldsymbol{u})$. The bilinear constraint is automatically satisfied for the entire IVP trajectory once the initial position consistent with Eq. (10) and "orthogonal" initial velocity in KS variables have been chosen. However, it is not automatically satisfied for the TPBVP. If one randomly chooses geometrically feasible initial and final $\boldsymbol{u}$ vectors, how do we also ensure "dynamic feasibility", in the sense that the initial and final $\boldsymbol{u}$ are actually the initial and final positions of the particular solution of Eq. (19)? There are an infinity of choices!

Due to the redundancy of the $\boldsymbol{u}$ space, two sets of admissible initial and final boundary conditions exist. As we show in the following, a one-parameter family of initial and final $\boldsymbol{u}$ points belong to each set, satisfying Eq. (10) at the initial and final times. It turns out there is a one-to-one correspondence of points in initial and final $\boldsymbol{u}$ space. Mapping the Cartesian coordinates into consistent initial and final $\boldsymbol{u}$ vectors is not trivial, because we find that each point in the feasible initial set flows into a specific point in the final set. Resolving the ambiguity introduced because an infinite set of $\boldsymbol{u}$ vectors geometrically correspond to a given (X, Y, Z) is a key aspect of the KS Lambert algorithm, in order to correctly specify terminal points that lie on the same dynamical path in $\boldsymbol{u}$ space. The final boundary conditions reside on a "fiber" [31] with a constant radius $(\sqrt{r_f})$ locating a point on the four-dimensional (4-D) sphere. The final boundary condition on this fiber cannot be determined analytically, as it is a function of the perturbed space through which the trajectory travels. Although we can resolve this problem completely for the case of planar motion where the space curve fiber degenerates into two distinct points, we must resort to numerical methods for general 4-D KS dynamics to implicitly select the proper final boundary condition. More on this is given in the following section.

Another interesting property of the KS transformation is $r = \boldsymbol{u}^T\boldsymbol{u}$, which is easily proven by squaring both sides of Eq. (10). Obviously, quadratic combinations of the elements of $\boldsymbol{u}$ produce the rectangular coordinates and the radial distance. The mapping from $\boldsymbol{u}$ to (X, Y, Z) is unique for all $\boldsymbol{u}$. However, the inverse from (X, Y, Z) to $\boldsymbol{u}$ [the rightmost equation of Eq. (10)] is not unique, and the given inverse transformation is the most popular of the set of inverse mappings.

It is well known that any transformed time coordinate that is linearly proportional to r, together with Eq. (10), maps the nonlinear differential equations [Eq. (9)] into four oscillators in $\boldsymbol{u}$ space. The nonlinearities vanish identically as $\boldsymbol{F} \to 0$. The $\boldsymbol{F}$ vector here is the Cartesian perturbing acceleration components augmented with a zeroth fourth element. We restrict attention in the present discussion to the case of perturbed elliptic orbits for which the instantaneous Keplerian energy ($\alpha = 1/a$) is positive, where $a = a(t)$ and we adopt the following implicit time transformation $E \to t$:

$$\frac{\mathrm{d}t}{\mathrm{d}E} = \left(\frac{1}{\sqrt{\mu\alpha}}\right) r, \qquad \alpha = \frac{2}{r} - \frac{\dot{\boldsymbol{r}}^T\dot{\boldsymbol{r}}}{\mu} \tag{13}$$

Note that

$$\frac{\mathrm{d}}{\mathrm{d}E} = \frac{\mathrm{d}}{\mathrm{d}t}\frac{\mathrm{d}t}{\mathrm{d}E}$$

so that, after some manipulation, we can show

$$\boldsymbol{u}' = \frac{\mathrm{d}\boldsymbol{u}}{\mathrm{d}E} = \frac{1}{2}\left[\sqrt{\mu\alpha}\right]^{-1} L^T(\boldsymbol{u})\dot{\boldsymbol{r}} \tag{14}$$

After considerable algebra, we derive the resulting differential equations:

$$\frac{\mathrm{d}^2\boldsymbol{u}}{\mathrm{d}E^2} + \frac{1}{4}\boldsymbol{u} = \frac{r}{2\mu\alpha}\left[I + \frac{4}{r}\frac{\mathrm{d}\boldsymbol{u}}{\mathrm{d}E}\frac{\mathrm{d}\boldsymbol{u}^T}{\mathrm{d}E}\right] L^T(\boldsymbol{u})\boldsymbol{F} \tag{15}$$

and time is related to the perturbed change in the eccentric anomaly from Eq. (13) through the integral

$$t = t_0 + \int_0^E \left(\frac{r(\theta)}{\sqrt{\mu\alpha(\theta)}}\right) \mathrm{d}\theta \tag{16}$$

Finally, for $\boldsymbol{F} \neq 0$, it can be shown that Eq. (22) α satisfies the variation-of-parameters differential equation

$$\frac{\mathrm{d}\alpha}{\mathrm{d}E} = -\frac{4}{\mu}\frac{\mathrm{d}\boldsymbol{u}^T}{\mathrm{d}E} L^T(\boldsymbol{u})\boldsymbol{F} \tag{17}$$

and the osculating energy in the classical Keplerian energy form of Eq. (13) can be transformed to the new form of the osculating constraint

$$\alpha = \frac{2}{r}\left[1 + \frac{4}{r}\frac{\mathrm{d}\boldsymbol{u}^T}{\mathrm{d}E}\frac{\mathrm{d}\boldsymbol{u}}{\mathrm{d}E}\right]^{-1} \tag{18}$$

The first expression for α [Eq. (13)] is the Cartesian form of the Keplerian energy equation, whereas the second expression [Eq. (18)] is the KS transformed Keplerian energy equation. This equation holds in the presence of perturbations for $\alpha(t)$ as an osculation constraint in the variation of parameters. Thus, α in Eq. (15) does not have to be solved by a differential equation as is frequently done. Rather it is a known function of the instantaneous KS state variables, given in Eq. (17). Notice E is the perturbed change in eccentric anomaly, and not the eccentric anomaly itself.

Substitution of the equation from Eq. (17) into Eq. (15) gives the new and elegant form for the generally perturbed differential equation of motion in the KS variables:

$$\frac{\mathrm{d}^2\boldsymbol{u}}{\mathrm{d}E^2} + \frac{1}{4}\boldsymbol{u} = \frac{r^2}{4\mu}\left[1 + \frac{4}{r}\frac{\mathrm{d}\boldsymbol{u}^T}{\mathrm{d}E}\frac{\mathrm{d}\boldsymbol{u}}{\mathrm{d}E}\right]\left[I + \frac{4}{r}\frac{\mathrm{d}\boldsymbol{u}}{\mathrm{d}E}\frac{\mathrm{d}\boldsymbol{u}^T}{\mathrm{d}E}\right] L^T(\boldsymbol{u})\boldsymbol{F} \tag{19}$$

Since the spherical harmonic series first term $1/r^2$ and all higher-order terms contain $1/r^n$, the multiplication by r^2 on the right-hand side (RHS) of Eq. (19) simply reduces by two the denominator powers of r in all the gravitational perturbations. In particular, for the second zonal harmonic, r^2 in the denominator of this second zonal harmonic perturbation is canceled. The formulation therefore has a regularizing effect on the dominant gravitational perturbation.

For an arbitrary force, differential equations (15–19) must be solved numerically; however, for small forces, they represent a weakly coupled, weakly nonlinear oscillator description of orbital motion, and these equations are attractive from several points of view. From the work of Bai and Junkins [6,4] and the classical Picard literature [5,11,12], we know that the convergence of the Picard method is a function of the "strength" of the dominant terms of the differential equation. Therefore, we can anticipate the $1/4$ coefficient of Eq. (15) and Eq. (19) suggests a basis for optimism that significant advantages will be achieved in these transformed differential equations, compared to Eq. (9), for reducing the number of Picard iterations and increasing the maximum interval over which the Picard contraction mapping iterations will converge. We anticipate these advantages for both the IVP and for the TPBVP. As will be evident in the following, these heuristic expectations are consistent with numerical reality and represent a significant computational advantage, especially for the Lambert problem.

In this section, we have derived a new form for the transformed equation of motion [Eq. (19)] in KS variables. By using the osculating constraint for α, we eliminate the need to solve the work/energy differential equation [Eq. (17)] for α, as is frequently done (with time variables that differ from E) in the classical references [28,29]. Thus, our KS differential equations are of order 9, and not 10, as is the case in the usual KS developments. In the following section, we formulate the Keplerian Lambert problem in KS variables. This is analogous to Battin's classical Lambert solution [1] but in new variables. Although formally analogous, our formulation here is not as general as Battin's. He considered all

species of conics (elliptical, parabolic, and hyperbolic) and, for the elliptic case, he considered the multiple revolution transfers as well. For this paper, we only consider the elliptical case. The universal generalizations are left for future developments. However, and importantly, we do generalize (in this paper) the Keplerian Lambert results to consider arbitrary smooth perturbations and demonstrate the formulation to solve perturbed TPBVPs using a (40, 40) spherical harmonic gravity model.

IV. Special Coordinate System

Now, let us consider the case of general perturbations. The two-point boundary value problem turns out to have some subtleties that arise due to the infinity of $\boldsymbol{u}$ vectors that correspond to given Cartesian coordinates. First, consider the three scalar equations implicit in Eq. (10):

$$X = u_1^2 - u_2^2 - u_3^2 + u_4^2 \quad Y = 2(u_1u_2 - u_3u_4)$$
$$Z = 2(u_1u_3 + u_2u_4) \tag{20}$$

Also, squaring Eq. (10) allows us to write

$$r = u_1^2 + u_2^2 + u_3^2 + u_4^2 \tag{21}$$

Adding the first of Eqs. (20) and (21) yields the nice result

$$u_1^2 + u_4^2 = R^2 = \frac{r + X}{2} \tag{22}$$

So, it is clear that (u_1, u_4) lie on a circle of radius $R = \sqrt{(r + X)/2}$, and so all infinity of possible (u_1, u_4) pairs can be parameterized by the angle

$$\phi = \tan^{-1}\left(\frac{u_4}{u_1}\right)$$

or

$$u_1 = R\cos\phi, \qquad u_4 = R\sin\phi, \qquad 0 \le \phi < 2\pi \tag{23}$$

Eliminating (u_1, u_4) as a function of ϕ, using Eq. (23) we can solve the second pair of Eqs. (20) simultaneously for (u_2, u_3) as

$$u_2 = \frac{1}{2R}(Y\cos\phi + X\sin\phi),$$
$$u_3 = \frac{1}{2R}(-Y\sin\phi + Z\cos\phi) \tag{24}$$

Equations (22–24) define a space curve or fiber on the surface of the four-dimensional sphere of radius $\sqrt{r}$. Sweeping ϕ over the 2π range generates all infinity of points along the fiber of feasible u_i coordinates corresponding to the given (X, Y, Z). There is one additional subtlety that turns out to offer a way to simplify the most general case. As is well known, the same Cartesian form of the equations of motion

$$\ddot{\boldsymbol{r}} = -\frac{\mu}{r^3}\boldsymbol{r} + \boldsymbol{F}$$

holds for an infinity of inertial Cartesian coordinate motion descriptions; therefore, we are free to choose the fixed inertial coordinate system orientation, so long as we are careful to project the force Cartesian components and boundary conditions appropriately into this chosen inertial frame. A classical orbit frame is defined by the initial position and velocity vectors as shown in Fig. 2. An alternate orbit frame is defined by the initial and final position vectors, as shown in Fig. 3. Notice, at either the initial or final time, that the boundary conditions, and therefore the preceding equations, simplify significantly if one of the inertial axes is aligned with either the initial or final position vector. It is also useful to rotate the inertial

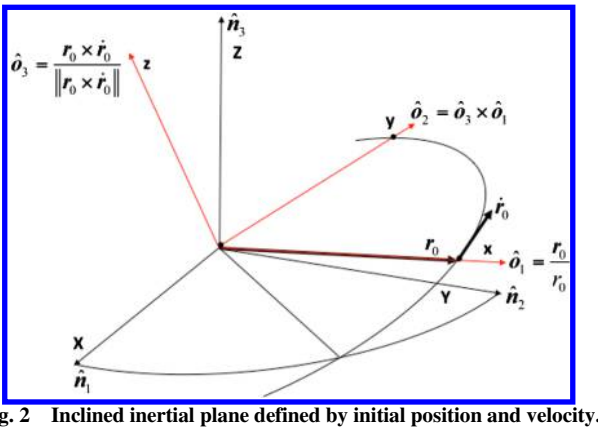

Fig. 2 Inclined inertial plane defined by initial position and velocity.

frame about the fixed axis so that the xy plane lies in the unperturbed plane of motion (e.g., Fig. 3). We can either use the initial position and velocity vector to define the special initial (xyz) plane or we can use (for two-point boundary value problems) the prescribed initial and final position vectors to define the inertial plane. For both cases, and for a small elapsed time, we can expect the out-of-plane motions to be small and, in some circumstances, this truth is useful to guide heuristics in applications.

As one example, if the inertial system is chosen such that the initial or final position vector aligns with the x axis such that $x = r$ and $y = z = 0$ at that point, then $R = \sqrt{r}$ and the aforementioned space curve assumes its simplest form as

$$u_1^2 + u_4^2 = r,$$
$$\{u_1 = \sqrt{r}\cos\phi, u_4 = \sqrt{r}\sin\phi\} \quad \text{and} \quad \{u_2 = 0, u_3 = 0\} \tag{25}$$

See Fig. 4 for a geometric interpretation of the mapping from Cartesian coordinates into the infinite set of $\{u_1, u_2, u_3, u_4\}$ coordinates, for this specific example. In this case, the locus of feasible vectors is a circle of radius $\sqrt{r}$ in the u_1, u_4 plane. This is one of the few examples where one can fully visualize a space curve in a four-dimensional space!

Notice, even though the infinite set of $\boldsymbol{u}$ vector boundary conditions exists for any given $\{X, Y, Z\}$, once $\boldsymbol{u}$ is selected, the corresponding velocity forward and inverse mappings of $(\dot{X}, \dot{Y}, \dot{Z})$ to $\boldsymbol{u}'$ are unique:

$$\begin{Bmatrix} \dot{X} \\ \dot{Y} \\ \dot{Z} \\ 0 \end{Bmatrix} = \frac{2\sqrt{\mu\alpha}}{r} L(\boldsymbol{u})\boldsymbol{u}' \Leftrightarrow \boldsymbol{u}' = \frac{r}{2\sqrt{\mu\alpha}} L^T(\boldsymbol{u}) \begin{Bmatrix} \dot{X} \\ \dot{Y} \\ \dot{Z} \\ 0 \end{Bmatrix} \tag{26}$$

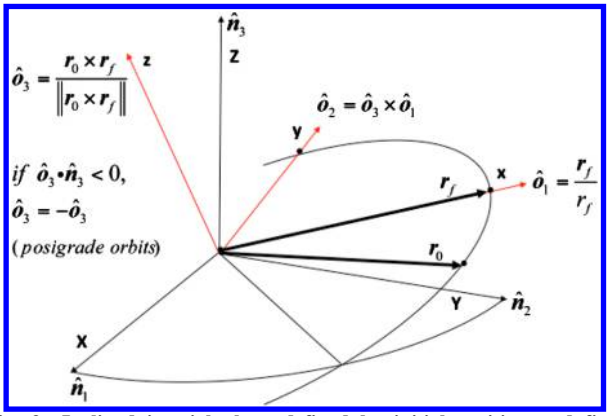

Fig. 3 Inclined inertial plane defined by initial position and final position.

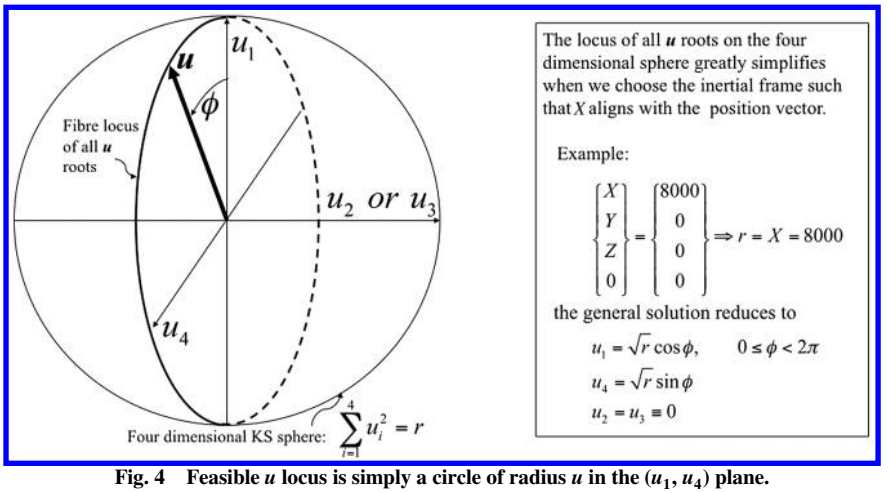

Fig. 4 Feasible u locus is simply a circle of radius u in the (u_1, u_4) plane.

The aforementioned developments can be used to resolve a key issue: Once an initial $\boldsymbol{u}$ vector is selected from among the infinity of possibilities, the corresponding velocity is computed from the second equation of Eq. (26), and then the solution of the KS differential [Eq. (19)] leads to a unique trajectory $(\boldsymbol{u}(\tau), \boldsymbol{u}'(\tau))$. Even if the initial $(\boldsymbol{u}(\tau), \boldsymbol{u}'(\tau))$ state is such that Eq. (10) gives the correct final Cartesian $\{X_f, Y_f, Z_f\}$, we need to focus on the truth that the arrival $\boldsymbol{u}(\tau(E_f))$ will correspond to only one of the infinity of $\boldsymbol{u}$ vectors consistent with $\{X_f, Y_f, Z_f\}$. So, when we attempt to prescribe an initial and final $\boldsymbol{u}$ vector to solve a TPBVP in $\boldsymbol{u}$ space, if we hold the initial $\boldsymbol{u}$ fixed, we must only determine the single unknown variable ϕ to correctly prescribe the terminal boundary condition for $\boldsymbol{u}(\tau(E_f))$ that mate the arrival state, of the unique MCPI Lambert solution of KS differential equation (19), with the boundary condition imposed at the initial time. Thus, a one-dimensional search over the set of feasible $\boldsymbol{u}$ boundary conditions is required to find ϕ that generates the particular $\boldsymbol{u}(\tau(E_f))$. However, through a judicious choice of the inertial frame, and using a warm start from Keplerian motion, we have been able to construct a reasonably efficient solution process having $\phi = 0$ if perturbations vanish, which evidently ensures the desired root for ϕ for the perturbed case is typically small. This enables algorithms to find the ϕ such that the initial and final boundary conditions in $\boldsymbol{u}$ space are the desired terminal states along the unique solution of the KS differential equations and correspond to the specified Cartesian terminal coordinates.

V. Analytical KS Lambert Solver

In this section, we develop a planar analytical KS Lambert solver that can be used as a warm start for solving the 4-D KS problem. The upper-left 2×2 submatrix of $L(\boldsymbol{u})$ is the needed subset of the position transformation, and the resulting equations simplify to the classical Levi-Civita transformation [1,32] discovered in 1920, which was some 40 years before the more general KS result [30]. Since the planar KS transformation reduces to a two-to-two mapping $(x, y) \Leftrightarrow (u_1, u_2)$, the root structure is greatly simplified and the fiber of solutions in 4-D reduce in two dimensions to fixed points (roots), as discussed in the following.

Restricting the motion to the plane $(z(t) = 0)$, the general KS transformation simplifies as follows:

$$\begin{Bmatrix} X \\ Y \end{Bmatrix} = L(\boldsymbol{u})\boldsymbol{u}, \quad \text{where } L(\boldsymbol{u}) = \begin{bmatrix} u_1 & -u_2 \\ u_2 & u_1 \end{bmatrix} \tag{27}$$

The inverse mapping is

$$\text{for } x \ge 0\text{: } \boldsymbol{u} = \pm \begin{Bmatrix} \left(\frac{(r+x)}{2}\right)^{1/2} \\ \frac{y}{(2(r+x))^{1/2}} \end{Bmatrix} \quad \text{or}$$

$$\text{for } x < 0\text{: } \boldsymbol{u} = \pm \begin{Bmatrix} \frac{y}{(2(r-x))^{1/2}} \\ \left(\frac{(r-x)}{2}\right)^{1/2} \end{Bmatrix} \tag{28}$$

As is evident in Eq. (10) and the planar special case of Eq. (27), the mapping from $\boldsymbol{u}$ space to Cartesian space is unique. As expected, the inverse mapping is not unique, but it is greatly simplified in two dimensions. In fact, for the planar case $(z(t) = 0)$, only two real points in $\boldsymbol{u}$ space exist, which are given in Eq. (28). For IVPs, as long as we avoid the potential division by zero at $x = \pm r$ [by following the sign of rules evident in Eq. (28)], the solution of these equations is very well behaved. For IVPs, we only need to use these equations once at initial time; and the inverse mapping in Eq. (27) [or, more generally, Eq. (10)] is nonsingular and unique everywhere. For TPBVPs, however, we have to resolve the sign ambiguities carefully; otherwise, we may accidentally request the algorithm to look for a one-and-a-fraction orbit transfer instead of a fractional orbit transfer. Note that two revolutions occur in Cartesian space for each revolution in $\boldsymbol{u}$ space, which is quite analogous to the quaternion representation of rotational motion.

For a given set of boundary conditions, there are two possible solutions that depend on the sign of the final position in $\boldsymbol{u}$ space. If the angle between the initial and final boundary conditions is less than π and the number of revolutions is odd (a fraction of the first orbit is considered an odd revolution and a fraction of the second orbit is considered an even revolution), then there is no sign change on the final position. However, in the odd orbits, when there is more than an angle of π between the initial and final positions, there is a sign change on the final boundary condition. The opposite sign convention occurs for an even orbit. For retrograde orbits, the aforementioned sign convention holds, but it is all reversed. Thus, for a fractional transfer angle of less than π in an odd revolution, we need to apply a sign change.

Using the planar KS transformation (Levi-Civita transformation), it is evident that solving the four uncoupled harmonic oscillators of Eq. (15) or Eq. (19) (where $\boldsymbol{F} = 0$) has an analytical solution simply given by

$$\begin{aligned} \boldsymbol{u} &= \boldsymbol{u}_0 \cos\frac{E}{2} + 2\frac{\mathrm{d}\boldsymbol{u}}{\mathrm{d}E}\bigg|_0 \sin\frac{E}{2}, \\ \frac{\mathrm{d}\boldsymbol{u}}{\mathrm{d}E} &= -\frac{1}{2}\boldsymbol{u}_0 \sin\frac{E}{2} + \frac{\mathrm{d}\boldsymbol{u}}{\mathrm{d}E}\bigg|_0 \cos\frac{E}{2} \end{aligned} \tag{29}$$

Or, in state transition matrix form,

$$\begin{Bmatrix} \boldsymbol{u} \\ \frac{\mathrm{d}\boldsymbol{u}}{\mathrm{d}E} \end{Bmatrix} = \begin{bmatrix} \Phi_{11} & \Phi_{12} \\ \Phi_{21} & \Phi_{22} \end{bmatrix} \begin{Bmatrix} \boldsymbol{u}_0 \\ \frac{\mathrm{d}\boldsymbol{u}}{\mathrm{d}E}\big|_0 \end{Bmatrix} \tag{30}$$

where the submatrices are $\Phi_{11} = \cos\frac{E}{2} I$, $\Phi_{12} = 2\sin\frac{E}{2} I$, $\Phi_{21} = -\frac{1}{2}\sin\frac{E}{2} I$, $\Phi_{22} = \cos\frac{E}{2} I$.

The integral of Eq. (16) can be carried out analytically for the $\boldsymbol{F} = 0$ case to obtain

$$\alpha^{3/2}\sqrt{\mu}(t - t_0) = E - (1 - \alpha r_0)\sin E - \alpha^{1/2}\sigma_0(\cos E - 1),$$
$$\sqrt{\mu}\sigma_0 \equiv \boldsymbol{r}_0 \cdot \dot{\boldsymbol{r}}_0 \tag{31}$$

where E denotes the change in the classical eccentric anomaly from initial conditions to the current state; i.e., herein, E is not referenced to perigee but rather to initial position. There is a single unique orbit for the fractional orbit transfer case, except for the colinear position case in which the orbit plane is not unique. The singularity structure for the Keplerian special case has been found to carry over to the gravitationally perturbed generalization of this two-point boundary value problem. The preservation of the singularity structure in the presence of perturbations is a consequence of the geometric truth that the osculating orbit plane is undetermined when the initial and final position vectors are colinear.

From Eq. (29), we can eliminate initial velocity in $\boldsymbol{u}$ space as a function of the final boundary conditions:

$$\frac{\mathrm{d}\boldsymbol{u}}{\mathrm{d}E}\bigg|_0 = \frac{1}{2\sin(E_f/2)}\left(\boldsymbol{u}_f - \boldsymbol{u}_0\cos\frac{E_f}{2}\right) \tag{32}$$

We now outline the completion of the solution of the Keplerian Lambert's problem in KS variables. Using the energy equation

$$\alpha = \frac{2}{r_0} - \frac{\mathrm{d}\boldsymbol{r}^T}{\mathrm{d}t}\bigg|_{t_0}\frac{\mathrm{d}\boldsymbol{r}}{\mathrm{d}t}\bigg|_{t_0} = \frac{2}{r_0}\left[1 + \frac{4}{r_0}\frac{\mathrm{d}\boldsymbol{r}^T}{\mathrm{d}E}\bigg|_{t_0}\frac{\mathrm{d}\boldsymbol{r}}{\mathrm{d}E}\bigg|_{t_0}\right]^{-1} \tag{33}$$

and Eq. (32), we can eliminate α and $\sigma_0 = \boldsymbol{r}_0 \cdot \dot{\boldsymbol{r}}_0/\sqrt{\mu}$ in Eq. (31) as a function of $(\boldsymbol{u}_0, \boldsymbol{u}_f, E_f)$, leaving only E_f as an unknown. Then, the modified Eq. (31) with all unknowns on the RHS is eliminated, except E_f can be iterated via a Newton/secant method to converge on the correct final eccentric anomaly E_f for a given final time t_f. An initial guess for the final eccentric anomaly is computed from the true anomaly using the dot product of the initial and final position vectors.

This method is well behaved, and convergence is reliable. For our application, we consider only fractional orbit cases. The efficiency of the KS Lambert solver is comparable (computation time is negligibly different) to that of the p iteration [2], which is an analytical Lambert solver in Cartesian variables (Fig. 5). Solving Lambert's problem analytically not only provides the final eccentric anomaly (corresponding to the final time) but also a warm start solution approximation for solving the perturbed problem.

It may seem that the warm start developed previously would only work for planar orbits; however, we can use this for any inclined orbit in three-dimensional (3-D) Cartesian space or 4-D $\boldsymbol{u}$ space. We construct a plane defined by the initial and final positions and use the corresponding constant direction cosine matrix to project the initial Cartesian coordinates from the equatorial frame into this special inertial frame. The warm start is computed in this special orbit frame, where $z = 0$ and $u_3 = u_4 = 0$.

Our KS Lambert solver is somewhat analogous to Battin's classical Lambert solution [1] but in new variables. Although, for geometrical clarity and to address the most common applications, we have developed these results for the elliptic (positive α case). It is clear that by following the pattern of [30], and especially [28], a universal analogy of the aforementioned developments can be developed that is applicable to all species of elliptical, parabolic, and hyperbolic motions. We leave this generalization for some future paper.

The present KS analytical solution of the Keplerian Lambert problem can virtually, certainly be improved upon. It is computationally competitive with the p iteration, which is not as efficient as other methods in terms of the iteration efficiency. However, our ultimate goal here is the development of generalized Lambert methods that accommodate rather general perturbations for which the classical Lambert algorithms do not apply. The present KS Lambert Keplerian solution should be viewed as a demonstration and not as the final word, but it does set the stage for the perturbed Lambert algorithms in the following in KS space.

VI. Theoretical Convergence

The domain over which the MCPI-IVP will converge is finite, and this gives rise to easily solvable challenges when the desired time interval over which a solution is sought is greater than the domain of convergence. For the TPBVP, Bai [3] also studied MCPI convergence and found that the interval was typically about one order of magnitude smaller for the TPBVP compared to the corresponding IVP. Bai and Junkins [4] did MCPI convergence analysis using a simple linear oscillator to provide some insight on the matter. We reiterate the key points of their study here, for reader convenience, and extend it to investigate the convergence domain (time-of-flight interval between the specified terminal positions) for the KS transformed equations of motion.

Consider a TPBVP described by the following equation, where c is a scalar:

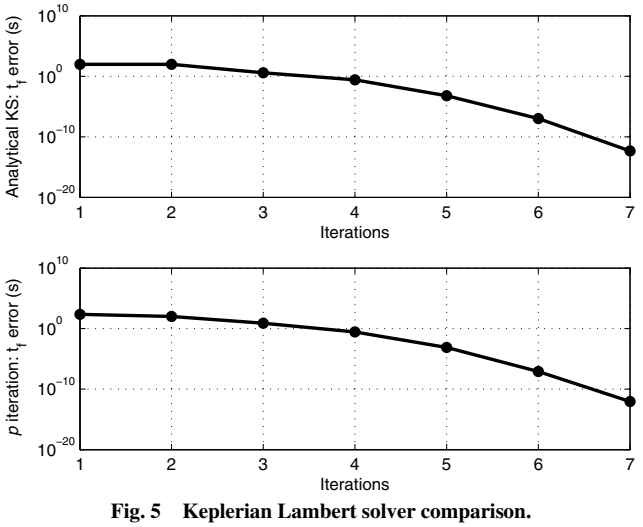

Fig. 5 Keplerian Lambert solver comparison.

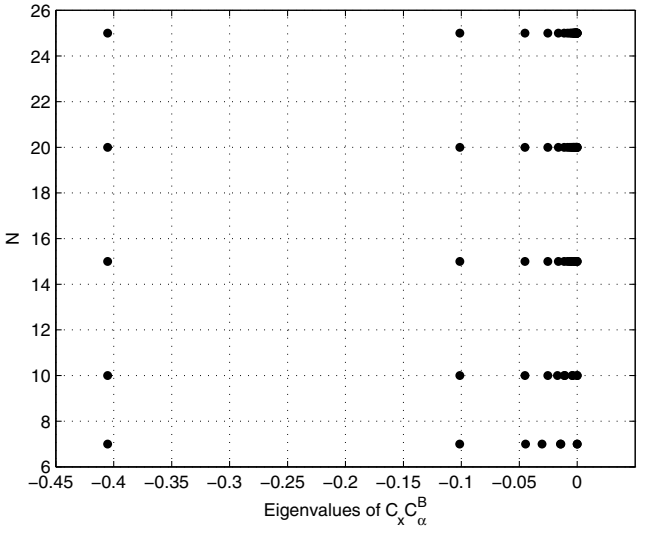

Fig. 6 TPBVP: eigenvalues of $C_x C_\alpha^B$.

Table 1 Test case orbits

Orbit type	Semimajor axis a, km	Eccentricity e
LEO	8,000	0.125
MEO	10,963	0.4
GTO	26,352	0.6
HEO	26,554	0.72

$$\frac{\mathrm{d}^2\boldsymbol{x}(t)}{\mathrm{d}t^2} = c\boldsymbol{x}(t), \qquad t\epsilon[t_0, t_f], \qquad \boldsymbol{x}(t_0), \qquad \boldsymbol{x}(t_f) = \boldsymbol{x}_f \tag{34}$$

This can be solved iteratively using the following equation, which is obtained from the procedure given in Fig. 1. A full derivation is presented in [3].

$$\boldsymbol{X}^{k+1} = cw_2^2 C_x C_\alpha^B \boldsymbol{X}^k + C_x \Theta_{xif}, \qquad w_2 = \frac{t_f - t_0}{2} \tag{35}$$

It is known from linear systems theory that this sequence is convergent to a fixed point only if all the eigenvalues of the matrix $[cw_2^2 C_x C_\alpha^B]$ are contained within the unit circle. That is, Eq. (35) must be a contraction mapping for convergence to a fixed point. The eigenvalues of $C_x C_\alpha^B$ for various N are shown in Fig. 6. In contrast [4] to the complex eigenvalues for the IVP that are attracted to fixed points on a small circle near the origin, inside the unit sphere, the real eigenvalues of $C_x C_\alpha^B$ for the case of a TPBVP are attracted to fixed points on a straight line inside the unit circle. The maximum magnitude of eigenvalues of $\lambda_{\max}(C_x C_\alpha^B)$ is almost invariant, for large N approaches a constant $\lambda_{\max}(C_x C_\alpha^B) \approx 0.4053$ with respect to increasing the Chebyshev order.

The necessary condition for convergence is given by

$$cw_2^2 \lambda_{\max}(C_x C_\alpha^B) \le 1 \tag{36}$$

Rearranging this with the unknown quantities on the left and known quantities on the right gives the following:

$$c(t_f - t_0)^2 \le \frac{4}{\lambda_{\max}(C_x C_\alpha^B)} \le \frac{4}{0.4053} \approx 9.87 \tag{37}$$

It is clear that the time interval and the linear coefficient c will dictate the domain over which the method will converge. Satisfying this condition guarantees that the Picard iteration will converge, for a fixed N, but it does not guarantee that N is sufficiently large to accurately approximate the solution. That is, although the solution will converge to some specific approximation, more nodes may be required to accurately capture the system dynamics with desired precision. Although still theoretically convergent, as the left-hand sides of Eqs. (36, 37) approaches the RHSs, the eigenvalues approach the stability boundary of the unit circle and very near the unit circle, and the convergence may be too slow to be considered practically convergent.

Performing the same analysis for the KS transformed equations of motion results in the following necessary condition for convergence:

$$\frac{1}{4}(E_f - E_0)^2 \le \frac{4}{0.4053} \approx 9.87 \tag{38}$$

Note that the c in Eq. (37) is replaced by $\frac{1}{4}$ in Eq. (38). To investigate how this affects convergence, we computed the theoretical domain of convergence for the four test case orbits given in Table 1.

Although this convergence analysis is formulated for linear systems, we use it on the nonlinear orbit equations [Eq. (39)] to simply provide some insight on what we can expect to see with regard to numerical convergence. The Keplerian orbit equations in Cartesian and KS variables are given as follows:

$$\ddot{\boldsymbol{r}} = -\frac{\mu}{r^3}\boldsymbol{r} \tag{39}$$

$$\boldsymbol{u}'' = -\frac{1}{4}\boldsymbol{u} \tag{40}$$

As an example, we compute the theoretical domain of convergence (in number of orbits) at perigee for the LEO given in Table 1. The local linear approximation of the equation means that the local c will vary around any noncircular the orbit. The smallest value for the domain of convergence would coincide with perigee, and thus should provide the most conservative guess.

At perigee,

$$t_f - t_0 \le \sqrt{\frac{4}{c\lambda_{\max}(C_x C_\alpha^B)}}$$

where, for a low-eccentricity orbit with $r_0 = 7000$ km, we adopt the approximation:

$$c \cong \frac{\mu}{7000^3} = 1.1621 \times 10^{-6}$$

This results in a maximum time of flight of $t_f - t_0 \le 34745$ s. The approximate domain of convergence can then be computed as $(t_f - t_0)/P \le 0.4$ orbits, where $P = 2\pi\sqrt{a^3/\mu}$. For an elliptical orbit, we find that basing this approximation on (r_0 = perigee) perigee radius while using an actual semimajor axis (a) proves conservative. If we do the same computation for the KS problem, we get

$$E_f - E_0 \le \sqrt{\frac{4}{c\lambda_{\max}(C_x C_\alpha^B)}}$$

where $c = \frac{1}{4}$. Therefore, $E_f - E_0 \le 6.28$ rad $= 2\pi$, and the theoretical domain of convergence when integrating KS variables is one orbit.

The preceding computation is done for the other test case orbits, and all the theoretical results are displayed in Fig. 7. Note that the theoretical convergence upper bound on transfer time, when solving the Keplerian Lambert problem by MCPI in Cartesian variables, decreases with increasing eccentricity. This is not the case in KS variables and, in fact, all orbits theoretically have the same MCPI domain of convergence (about one orbit), regardless of eccentricity.

Of course, this discussion is qualitative, since equations of motion in Cartesian coordinates are nonlinear and rigorous local linearization will cause the effective c to vary around the orbit, and the theoretical value computed previously does not rigorously represent the attainable convergence. However, we have done numerical studies that show that these theoretical bounds agree within about 15% in predicting the upper-bound time interval over which the MCPI can achieve practical convergence. In KS

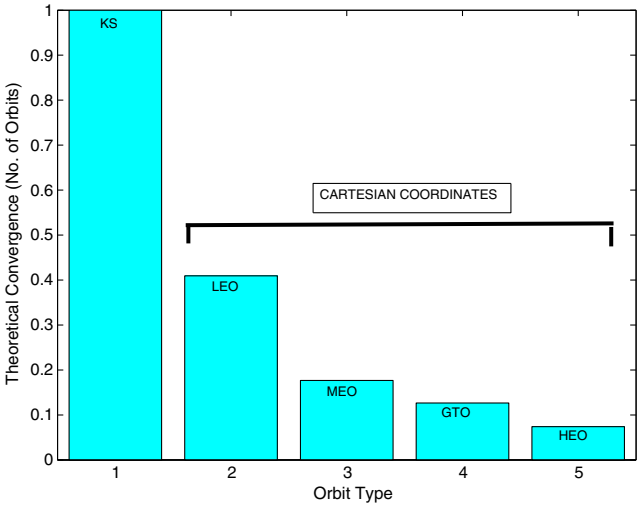

Fig. 7 TPBVP theoretical convergence.

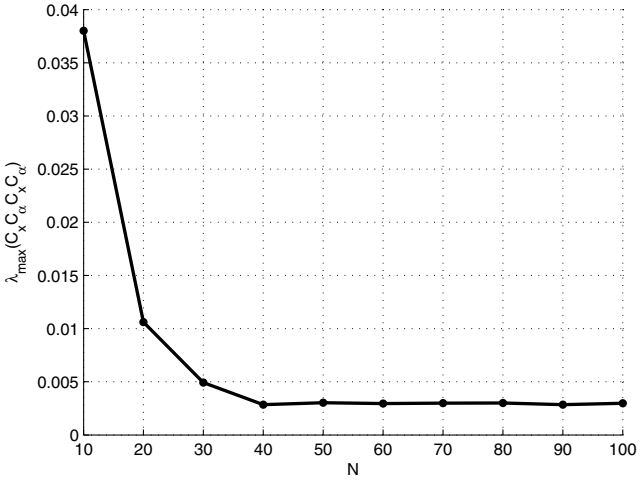

Fig. 8 IVP: Maximum eigenvalues of $C_xC_\alpha C_xC_\alpha$.

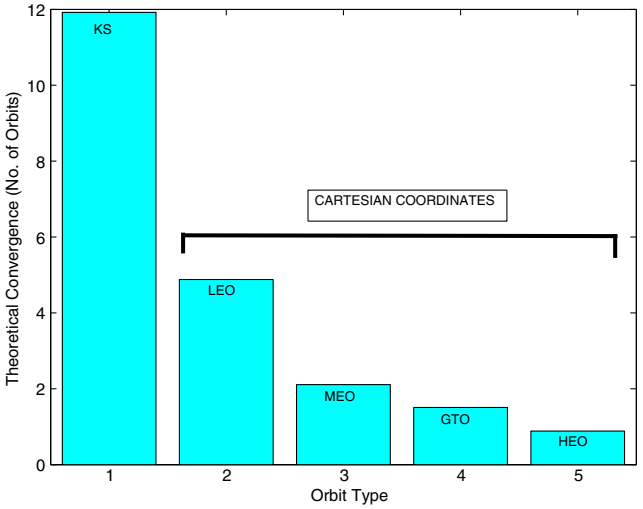

Fig. 9 IVP theoretical convergence.

coordinates, the motion is linear without approximation and $c = \frac{1}{4}$ is rigorously constant. Based on this theoretical analysis, it is clear that the KS transformation is extremely powerful when the resulting regularized differential equations are solved by MCPI.

Having considered the MCPI-TPBVP, we conduct the same analysis for the MCPI-IVP. The necessary condition for convergence is shown in the following, with the maximum eigenvalues of $[C_xC_\alpha C_xC_\alpha]$ displayed in Fig. 8:

$$\left|c(t_f - t_0)^2\right| \leq \frac{4}{\lambda_{max}(C_xC_\alpha C_xC_\alpha)} \leq \frac{4}{0.003} \approx 1300 \qquad (41)$$

The theoretical domain of convergence for the IVP is presented in Fig. 9. It is interesting to note that the theoretical domain of convergence for the MCPI-IVP is much greater than that for the MCPI-TPBVP and, in KS variables, the domain of convergence is increased for both the IVP and TPBVP compared with that achievable in Cartesian variables. In the following sections, we compute the domain of convergence numerically and anticipate that these insightful theoretical results will be an optimistic estimate of the truth.

VII. Keplerian Lambert Problem Solver by MCPI: Cartesian Versus KS

To study the numerical domain of convergence for Lambert's problem, we use the MCPI-TPBVP implementation to integrate the

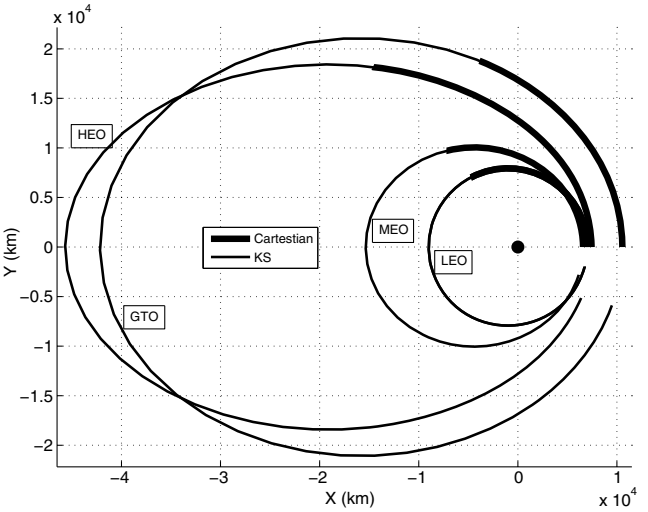

Fig. 10 MCPI domain of convergence comparison: Cartesian vs KS.

Keplerian equations of motion in both Cartesian and KS variables. The four test cases given in Table 1, with varying semimajor axes and eccentricities, span the region of interest. We anticipate that the Keplerian MCPI results will provide an indication of the ideal range of convergence associated with perturbations, and these results will show how much the introduction of perturbations "costs" in terms of reduction of the convergence domain. In all cases, the Hamiltonian is preserved to machine precision.

Figure 10 shows the results for these four orbits. In each test case, the thin solid line and thick solid line represent the domain of convergence for the problem solved using KS and Cartesian variables, respectively. It is clear that implementing the KS transformation has enabled the domain of convergence to be vastly improved relative to the usual Cartesian coordinate formulation: from a small fraction of an orbit (about one-third) to almost a full orbit. These numerical results agree relatively well with the predicted theoretical results.

These results simply demonstrate the superiority, with regard to convergence, of the MCPI-TPBVP implementation in KS variables compared with that in Cartesian variables. Since we already have analytic methods (except for iteration of a single transcendental equation) for solving the Keplerian Lambert problem (for example, Battin's method [1], the p iteration, and our KS Lambert solver presented in the previous section), there is no evident advantage to solve the Keplerian problem using MCPI. However, when considering the perturbed problem, which is discussed in the following sections, integrating the perturbed KS equations of motion becomes an extremely useful and very efficient compared with other methods. As a final observation using segmentation, the MCPI algorithm for the IVP can propagate orbits over arbitrarily long time intervals. However, for the boundary value problem (BVP), if we wish to avoid shooting methods, the maximum interval over which MCPI converges is a very important issue. It is evident that, for up to 95% of an orbit, all fractional orbit Keplerian Lambert transfers can be solved by MCPI (no linearization based shooting method is required) and, in the following developments, we show this holds true for the gravitationally perturbed Lambert problem with a modest reduction in the maximum time interval for convergence. Even with the KS formulation, for the multirevolution orbit transfers, we must resort to nonlinear shooting algorithms.

VIII. Perturbed Lambert Problem: KS Versus Cartesian

We now generate the formulation to consider perturbations. As mentioned in a previous section, the MCPI-TPBVP is not a Newton-like shooting method and is advantageous from the point of efficiency. However, solving a TPBVP requires specifying both the initial and final positions. These are known in Cartesian space and can

be converted to KS space. However, it is readily verified that the final boundary condition in the perturbed $\boldsymbol{u}$ space is not unique. This presented several challenges, which we will discuss in the following along with our method and algorithm for solving this unique problem.

Reflection on the truth that at every instantaneous point along a Cartesian trajectory $(X(t), Y(t), Z(t))$, there is an instantaneous sphere of radius $\sqrt{r} = \boldsymbol{u}^T\boldsymbol{u}$ in $\boldsymbol{u}$ space that contains the geodesic of Eq. (25). This instantaneous geodesic contains all the feasible $\boldsymbol{u}$ points consistent with the projection $\boldsymbol{r} = L(\boldsymbol{u})\boldsymbol{u}$. Notice that a particular unique trajectory for $(\boldsymbol{u}(E), \boldsymbol{u}'(E))$ ensues from solving KS differential equation (15) with the initial conditions

$$\boldsymbol{u}(0) = \frac{1}{r_0} L^T(\boldsymbol{u}(0))\boldsymbol{r}_0 \quad \text{and} \quad \boldsymbol{u}'(0) = \frac{r_0}{2\sqrt{\mu\alpha_0}} L^T(\boldsymbol{u})\dot{\boldsymbol{r}}_0 \tag{42}$$

Note that $\boldsymbol{u}'(0)$ cannot now be chosen independently of $\boldsymbol{u}(0)$ because admissible $\boldsymbol{u}'(0)$ must satisfy $L_4(\boldsymbol{u}(0))\boldsymbol{u}'(0) = 0$. Associated with $\boldsymbol{u}(E)$, there is a specific $\phi(E)$ consistent with the instantaneous $\boldsymbol{u}_1(E)$ and $\boldsymbol{u}_4(E)$, viz,

$$\tan(\phi(E)) = \frac{\boldsymbol{u}_4(E)}{\boldsymbol{u}_1(E)}$$

Thus, the time-varying sphere of radius $\sqrt{r(E)}$ sweeps out a four-dimensional tube in $\boldsymbol{u}$ space that initiates with a radius $\sqrt{r_0}$ and terminates with a final radius $\sqrt{r_f}$. Also, the geodesic curve gives the feasible $\boldsymbol{u}(E)$ corresponding to $(X(t), Y(t), Z(t))$, located at a point on the instantaneous sphere of radius $\sqrt{r}$ completely defined by the angle

$$\phi(0) = \tan^{-1}\left(\frac{\boldsymbol{u}_4(0)}{\boldsymbol{u}_1(0)}\right)$$

which is an angle in the $\boldsymbol{u}_1(0), \boldsymbol{u}_4(0)$ plane. Traditionally, the specific choice of $\phi_0 = 0$ is made. Note that, for general 3-D perturbed motion, we cannot constrain $\phi(E) = 0$ along the $\boldsymbol{u}$ trajectory because $\phi(E) = \tan^{-1}(\boldsymbol{u}_4(E)/\boldsymbol{u}_1(E))$ must hold true. All of this is leading up to the key points: The desired solution $(\boldsymbol{u}(E), \boldsymbol{u}'(E))$ for a TPBVP has a specific $\phi(E)$ history that initiates with some arbitrary $\phi(0)$ and arrives with some specific $\phi(E_f) = \phi_f$. We will not know ϕ_f a priori. A key issue is finding ϕ_f so $\boldsymbol{u}(E_f)$ can be computed such that it lies on the solution of the KS differential equations. In the following, we discuss a few more preliminaries and a recipe that we have found reliably solves this problem.

Our method to solve this problem is a hybrid use of the MCPI-KS-TPBVP algorithm and the MCPI-KS-IVP. We solve the TPBVP in $\boldsymbol{u}$ space using the boundary conditions computed by transforming the Cartesian boundary conditions into $\boldsymbol{u}$ space:

$$\{\boldsymbol{u}_{\text{TPBVP}}(E), \boldsymbol{u}'_{\text{TPBVP}}(E), \phi_f\} = \text{KS}_{\text{TPBVP}}(\boldsymbol{u}_0, \boldsymbol{u}(E_f)) \tag{43}$$

where $\boldsymbol{u}(E_f)$ is the geodesic admissible fiber of final boundary conditions given by Eqs. (22) to (24), which is a point on the circle of radius $\sqrt{r_f}$ in Fig. 4:

$$\boldsymbol{u}(E_f) = g(x_f, 0, 0, \phi_f) \tag{44}$$

where g represents u_1, u_2, u_3, and u_4 given in Fig. 4. That is, $g()$ is the space curve for the special coordinate system.

Because we have a weakly perturbed problem, we anticipate that the warm start will be near the final solution; this produces an initial $\boldsymbol{u}$-space velocity $\boldsymbol{u}'$ that is close to the ultimate desired final velocity, but it slightly violates the bilinear constraint. Although the trajectory computed by the MCPI-KS-TPBVP meets the final boundary conditions, when converted back to Cartesian space, it has a small fourth component of velocity, which is not physically possible and is, of course, due to the bilinear constraint not being satisfied. To trim this fourth component, we convert $\boldsymbol{u}'$ into Cartesian velocity and just set the small fourth component equal to zero. We then convert this physically admissible Cartesian velocity back to the $\boldsymbol{u}$ space and input this now physically feasible KS velocity $\boldsymbol{u}'$ and the initial position boundary condition in $\boldsymbol{u}$ space into the MCPI-KS-IVP, as shown in the following:

$$\{\boldsymbol{u}_{\text{IVP}}(E), \boldsymbol{u}'_{\text{IVP}}(E), \phi(E_f)\} = \text{KS}_{\text{IVP}}(\boldsymbol{u}_0, \boldsymbol{u}'_0) \tag{45}$$

where

$$\boldsymbol{u}'_{\text{TPBVP}}(0) = \frac{r}{2\sqrt{\mu\alpha}} L(\boldsymbol{u}(0))\dot{\boldsymbol{r}}(0) \tag{46}$$

and

$$\phi_f = \frac{\boldsymbol{u}_{4_{\text{IVP}}}(E_f)}{\boldsymbol{u}_{1_{\text{IVP}}}(E_f)} \tag{47}$$

We evaluate the converged $\boldsymbol{u}$ trajectory for the desired time interval and find that the final boundary condition in $\boldsymbol{u}$ space is slightly perturbed from that which we originally prescribed on the plane. Figure 11 illustrates the geodesic curves and the initial and final

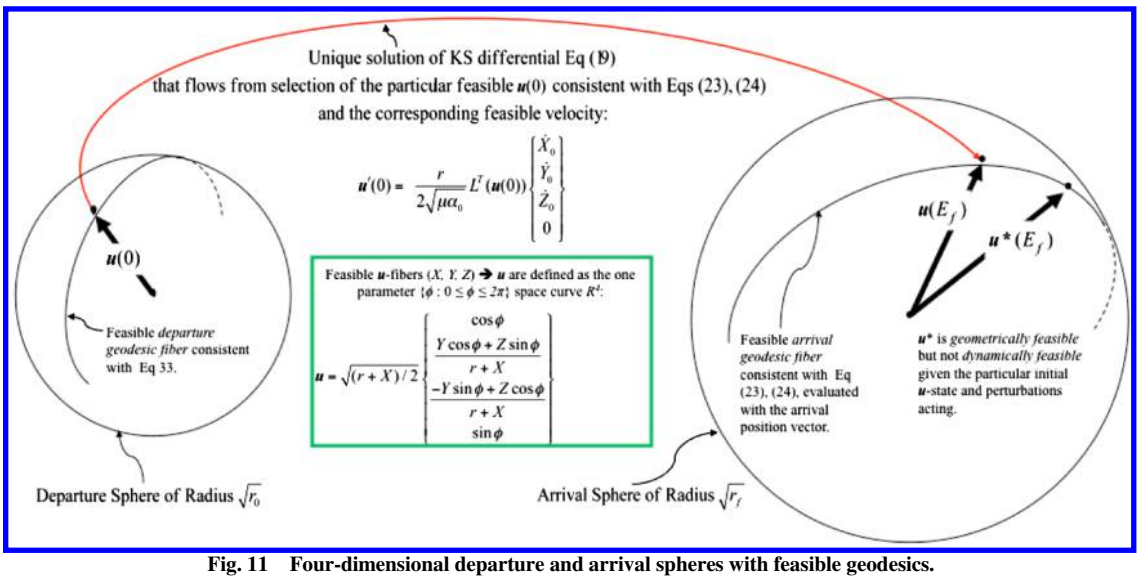

Fig. 11 Four-dimensional departure and arrival spheres with feasible geodesics.

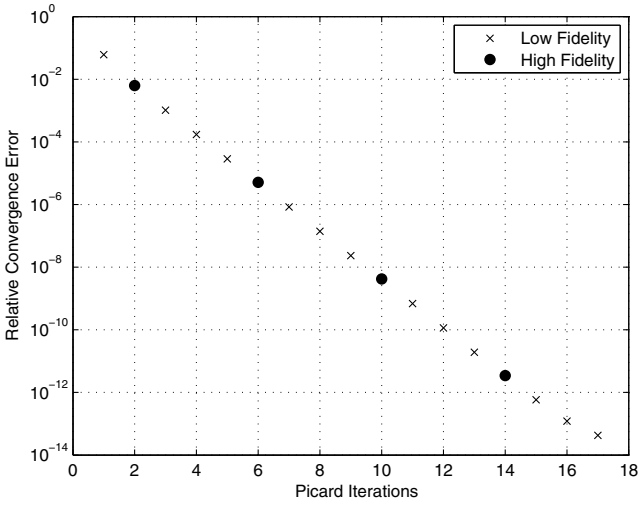

Fig. 12 Variable-fidelity gravity convergence pattern.

boundary conditions in perturbed $\boldsymbol{u}$ space. We use this new final boundary condition to compute ϕ_f, which we use to compute the new final position in $\boldsymbol{u}$ space. The MCPI-KS-TPBVP is run one more time with this new final boundary condition. Remarkably, the resulting solution has been found to reliably meet the initial and final boundary conditions in Cartesian space and to preserve the Hamiltonian to machine precision.

The perturbed Lambert's problem is solved with gravity perturbations, using the Earth gravitational model 2008 spherical harmonic gravity model [17]. As with the unknown final boundary condition discussed in the previous paragraphs, the final eccentric anomaly E_f corresponding to the final time t_f is also no longer analytically computable. Thus, we make use of the two-body final time (and final eccentric anomaly) computed with our analytical KS Lambert solver as an initial guess for solving the perturbed problem. The analytical KS Lambert solver also provides the two-body trajectory solution that is used as a warm start for solving the perturbed problem. It is advantageous to use this regularized KS warm start as opposed to a warm start generated using Battin's [1] (Cartesian) analytical solution, but either will work. Note that the node spacing should be chosen as an eccentric anomaly change and mapped onto -1 to 1, using cosine sampling, in order to facilitate efficient convergence of MCPI. Once the Picard iterations have converged, the final time (and final eccentric anomaly) is updated using the secant method. This Picard/secant sequence of iterations is repeated until the final solution satisfies both the specified time and Picard tolerances. Typically, about four or five secant iterations are required for convergence to the desired final time.

All of our perturbed MCPI-TPBVP algorithms makes use of a radially adaptive gravity approximation [19] and a variable fidelity force model [7]. While maintaining a machine precision Hamiltonian, these enhancements greatly increase the overall efficiency of our algorithms by reducing the number of "full" force function evaluations required for convergence. Figure 12 shows the typical variable fidelity convergence pattern, where the large dots represent the usual (full) force function evaluations and the crosses represent the low-fidelity force function evaluations. The decision about whether to use a local approximate gravity vs the global full model is based on a one-time study that "knew" the validity of the inexpensive local Taylor series as a function of the small displacement from the node location of the last neighboring full evaluation. More details on these local gravity approximations are given in [7,19].

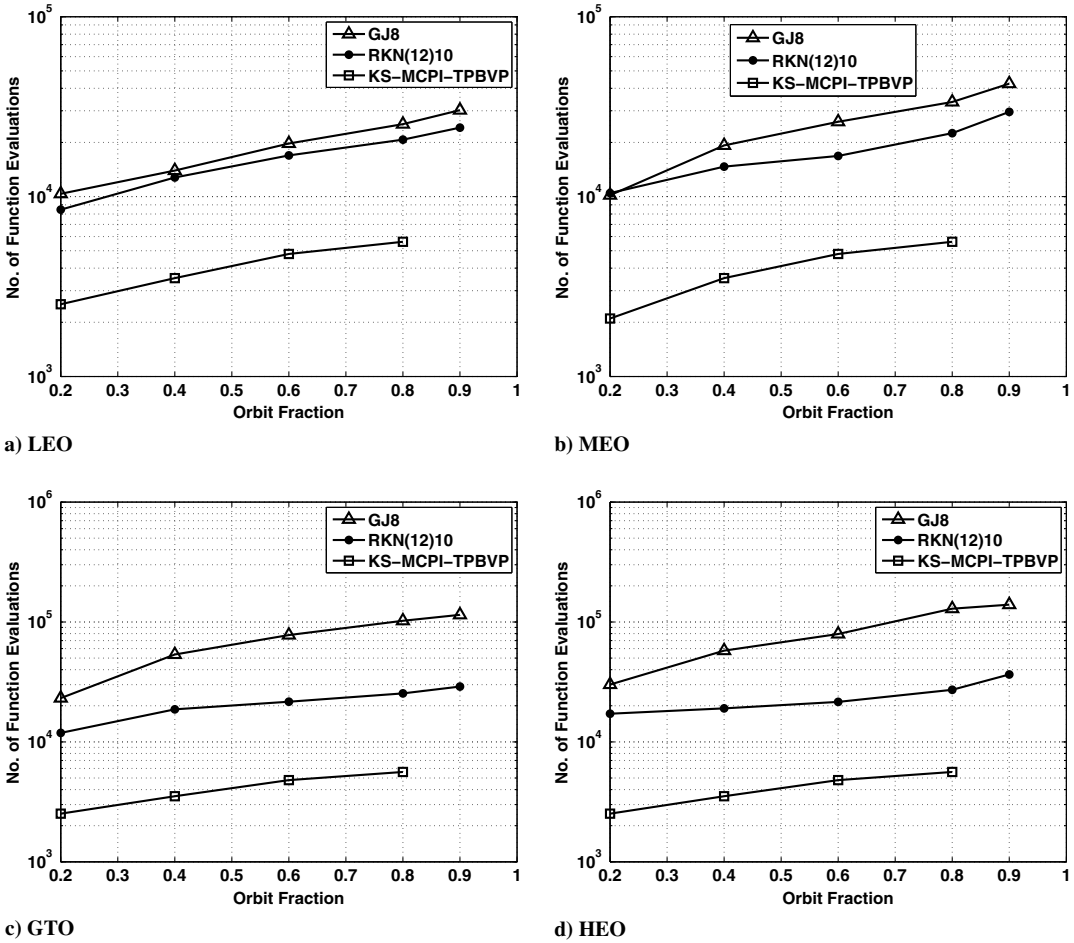

a) LEO **b) MEO**

c) GTO **d) HEO**

Fig. 13 Efficiency comparison of three methods for solving the perturbed Lambert problem.

To demonstrate the efficiency of our algorithm, we solve the test case orbits in Table 1 using MATLAB's *fsolve* where Runge–Kutta–Nystrom 12(10) [33] and Gauss–Jackson 8 [34] are the adopted integrators. In all cases, the methods were tuned to maintain a near-machine-precision Hamiltonian. The results reveal that our regularized MCPI-TPBVP/IVP algorithm is the most efficient method for solving the perturbed Lambert's problem over this interval: that is, over an interval that falls outside of the range attainable using the MCPI-TPBVP in Cartesian variables (about one-third of an orbit) and inside of the range attainable using the MCPI-TPBVP in KS variables (just short of 1 orbit). Figure 13 shows these results.

IX. Initial Value Problem: Cartesian Versus KS Equations of Motion Solved via MCPI

The KS transformation and Picard iteration can also be applied to solving initial value problems, in much the same way as the classical Cartesian differential equations have been solved by MCPI [27]. As expected, we find that the domain of convergence achievable for the IVP in KS variables is greatly increased compared with that in Cartesian variables. The KS implementation achieves practical convergence over eight orbits with no dependence on eccentric orbits, compared with the Cartesian implementation that ranges from about 1.5 to 4 orbits, depending on the eccentricity of the orbit. These numbers agree relatively well with the theoretical values computed in a previous section: more so for the Cartesian implementation than for the KS. The theoretical results predict about 12 orbits for the KS implementation; however, our experiments revealed that 2000 nodes are required for the trajectory to converge over eight orbits. That is, although the Picard method theoretically converges over such long time arcs, the number of basis functions required (greater than 2000) is usually not attractive. Numerical challenges begin to arise, and integrating the motion in "one segment" is not particularly efficient due to slowness of convergence as the eigenvalues approach the unit circle. Fractional orbit segmentation should be used in practice to reduce the number of iterations, and therefore drastically reduce the overall number of acceleration computations. A recent study by Macomber et al. [21] shows that three to five segments per orbit typically lead to optimal efficiency for Cartesian equations of motion. Typically, 10 or fewer Picard iterations are needed with a warm start over an optimal fraction of an orbit segments. Only one or two of these Picard iterations require the full force model. The fixed-point nature of convergence permits the use of local force approximations to make most of the local force computations extremely cheap compared to the full force model. Thus, the number of Picard iterations is not nearly as important as the number of effective full force computations at each node.

In solving the perturbed KS-IVP we make use of the optimal segmentation scheme [21] and also a two-body warm start. The final two-body eccentric anomaly is used as an initial guess to start the iterations. Unlike the perturbed Lambert problem, we do not require a secant method to solve for the final eccentric anomaly corresponding to the desired final time. Instead we solve the perturbed KS-IVP with the two-body final eccentric anomaly E_f plus 2% (we found that increasing E_f by 2% was conservative and ensured we integrate past the final time of interest). After convergence, it is easy to isolate any "real" E_f interior point corresponding to the chosen t_f by interpolation/iteration. A qualitative difference between this approach and that used for the perturbed Lambert's problem is that a repetitive Picard/secant iteration scheme is not required. For the IVP, the secant method is only required once, after the Picard iterations have converged, to isolate the final time of interest.

Looking at Figs. 14 and 15, we see that the KS transformation does have a slight advantage over the Cartesian IVP implementation, but it is not as significant as it is for Lambert's problem. When a variable-fidelity gravity model is applied, as was done for the perturbed Lambert's problem, we find that the number of full force evaluations required for the solution to converge to machine precision is the same for both the Cartesian and KS implementations. Thus, the benefit that the KS implementation provides is a saving of perhaps one or two low-fidelity force function evaluations per node.

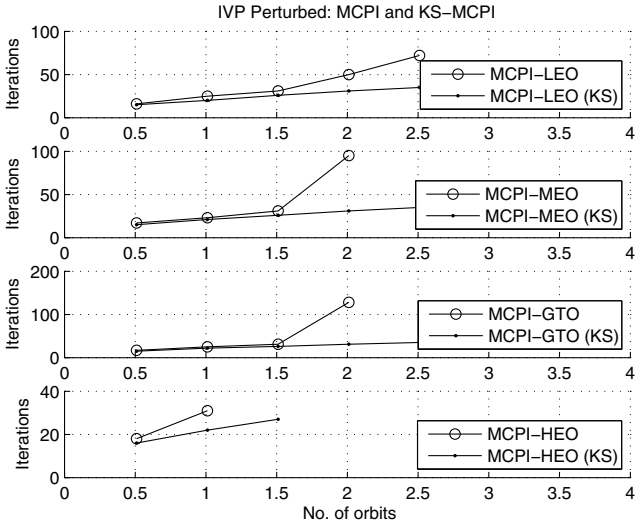

Fig. 14 MCPI IVP number of iterations required for convergence: Cartesian vs KS.

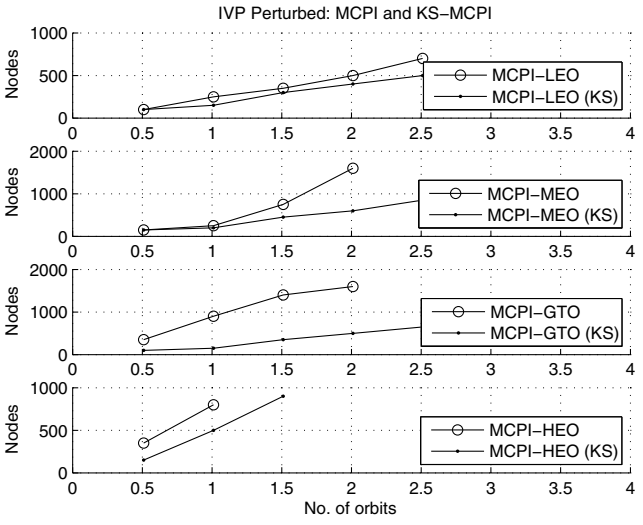

Fig. 15 MCPI IVP number of nodes required for convergence: Cartesian vs KS.

Using the KS transformation and MCPI for solving IVPs produces nice academic results; however, in reality, these do not provide a significant advantage over the already very efficient Cartesian IVP implementation of MCPI [7]. Pursuing this KS IVP analysis involved considerable work and enabled us to gain valuable insight about this problem. It is important that this (not what we anticipated or desired) outcome be documented in the event that others consider pursuing this same avenue. Although the KS MCPI transformed equations of motion did not show an advantage for solving the pure IVP, this method is required as part of the MCPI-KS-TPBVP algorithm with is presented in detail in the preceding section. As mentioned above, the advantage that the MCPI-KS-IVP/TPBVP solver provides is very significant.

X. Conclusions

A new algorithm for accurate and efficient solution of the perturbed Lambert problem was developed. This method combined the path approximation numerical integrator, the Modified Chebyshev–Picard iteration, and the Kustaanheimo–Stiefel regularizing time transformation. An analytical solution to the elliptic Keplerian Lambert problem was first developed based on Kustaanheimo–Stiefel (KS)

regularization, which transformed the nonlinear 3-D orbit equations of motion into four linear oscillators. Following this, an algorithm was developed to solve the elliptic Keplerian two-point boundary value problem (TPBVP) and initial value problem (IVP) using the KS transformation and Picard iteration. Solving the Keplerian TPBVP in KS variables via Modified Chebyshev–Picard iteration (MCPI) resulted in an increase in the practical domain of convergence from about one-third of an orbit (in Cartesian variables, for low eccentricity) to 95% of an orbit. For the Keplerian IVP, the domain of convergence of the Picard iteration increased to more than double that of the Cartesian IVP. These large increases in the domain of convergence were independent of orbital eccentricity. An algorithm to solve the perturbed elliptic TPBVP using the KS transformation and Picard iteration was also developed. To demonstrate the numerical efficiency of the approach, a (40,40) degree and order spherical harmonic gravity model was considered. Similar increases in the domain of convergence were observed for the perturbed TPBVP. The accuracy and efficiency of the current regularized MCPI-TPBVP algorithm for solving the perturbed Lambert's problem were shown superior to MATLAB's *fsolve*, where RKN12(10) and Gauss–Jackson were the integrators used for comparison. This paper provides a general treatment of Lambert's problem in KS coordinates and, in this sense, completes an important set. The algorithms promise to have an impact on practical problems, since general perturbations and high precision are efficiently accommodated.

Acknowledgments

We thank our sponsors U.S. Air Force Office of Scientific Research (Julie Moses), U.S. Air Force Research Laboratory (Alok Das and staff Paul Schumacher), and Applied Defense Solutions (Matt Wilkins) for their support and collaborations under various contracts and grants. We acknowledge many productive conversations and contributions made by members of the Texas A&M Astrodynamics team: K. T. Alfriend, John Hurtado, James Turner, Xiaoli Bai, Kohei Fujimoto, Tarek Elgohary, Brent Macomber, Austin Probe, and Julie Read.

References

[1] Battin, R., *An Introduction to the Mathematics and Methods of Astrodynamics*, AIAA Education Series, AIAA, Reston, VA, 2014, pp. 276–281, 295–342.

[2] Schaub, H., and Junkins, J., *Analytical Mechanics of Aerospace Systems*, 3rd ed., AIAA Education Series, AIAA, Reston, VA, 2014, pp. 666–672.

[3] Bai, X., "Modified Chebyshev–Picard Iteration Methods for Solution of Initial Value and Boundary Value Problems," Ph.D. Dissertation, Texas A&M Univ., College Station, TX, 2010.

[4] Bai, X., and Junkins, J., "Modified Chebyshev–Picard Iteration Methods for Solution of Boundary Value Problems," *Advances in the Astronautical Sciences*, Vol. 58, No. 4, Oct.–Dec. 2011, pp. 615–642. doi:10.1007/BF03321534

[5] Clenshaw, C. W., and Norton, H. J., "The Solution of Nonlinear Ordinary Differential Equations in Chebyshev Series," *Computer Journal*, Vol. 6, No. 1, 1963, pp. 88–92. doi:10.1093/comjnl/6.1.88

[6] Bai, X., and Junkins, J., "Modified Chebyshev–Picard Iteration Methods for Solution of Initial Value Problems," *Advances in the Astronautical Sciences*, Vol. 58, Nos. 1–2, Jan.–June 2012, pp. 335–359.

[7] Probe, A., Macomber, B., Kim, D., Woollands, R., and Junkins, J., "Terminal Convergence Approximation Modified Chebyshev–Picard Iteration for Efficient Numerical Integration of Orbital Trajectories," *Advanced Maui Optical Space Surveillance Technologies Conference*, Maui, HI, 2014.

[8] Woollands, R., Bani Younes, A., Macomber, B., Probe, A., Kim, D., and Junkins, J., "Validation of Accuracy and Efficiency of Long-Arc Orbit Propagation Using the Method of Manufactured Solutions and the Round-Trip-Closure Method," *Advanced Maui Optical Space Surveillance Technologies Conference*, Maui, HI, 2014.

[9] Probe, A., Macomber, B., Woollands, R., Masher, A., Read, J., Jones, B., and Junkins, J., "Benchmark Problems for Numerical Astrodynamics Propagation Algorithms," *Computer Modeling in Engineering Sciences* (submitted for publication).

[10] Woollands, R., Masher, A., Macomber, B., Probe, A., Kim, D., Read, J., Bani Younes, A., and Junkins, J., "Modified Chebyshev–Picard Iteration Accuracy and Stability for Multi-Orbit Propagation," *Computer Modeling in Engineering Sciences* (submitted for publication).

[11] Feagin, T., "The Numerical Solution of Two Point Boundary Value Problems Using the Chebyshev Polynomial Series," Ph.D. Thesis, Univ. of Texas, Austin, TX, 1972.

[12] Shaver, J., "Formulation and Evaluation of Parallel Algorithms for the Orbit Determination Problem," Ph.D. Dissertation, Dept. of Aeronautics and Astronautics, Massachusetts Inst. of Technology, Cambridge, MA, 1980.

[13] Fukushima, T., "Vector Integration of Dynamical Motions by the Picard-Chebyshev Method," *Astronomical Journal*, Vol. 113, June 1997, pp. 2325–2328. doi:10.1086/118443

[14] Junkins, J., Bani Younes, A., Woollands, R., and Bai, X., "Orthogonal Approximation in Higher Dimensions: Applications in Astrodynamics," *JN Juang Astrodynamics Symposium*, American Astronomical Soc. Paper 12-634, Washington, D.C., 2012.

[15] Junkins, J., Bani Younes, A., Woollands, R., and Bai, X., "Orthogonal Approximation in Higher Dimensions: Applications in Astrodynamics," *Journal of the Astronautical Sciences*, Dec. 2012.

[16] Junkins, J., Bani Younes, A., Woollands, R., and Bai, X., "Picard Iteration, Chebyshev Polynomial and Chebyshev–Picard Methods: Application in Astrodynamics," *Journal of the Astronautical Sciences*, Dec. 2012. doi:10.1007/s40295-015-0061-1

[17] Bani Younes, A., "Orthogonal Polynomial Approximation in Higher Dimensions: Applications in Astrodynamics," Ph.D. Dissertation, Texas A&M Univ., College Station, TX, 2013.

[18] Macomber, B., Woollands, R., Probe, A., Bani Younes, A., and Junkins, J. L., "Modified Chebyshev–Picard Iteration for Efficient Numerical Integration of ordinary Differential Equations," *Advanced Maui Optical and Space Surveillance Technologies Conference*, 2013.

[19] Probe, A., Macomber, B., Read, J., Woollands, R., and Junkins, J., "Radially Adaptive Evaltuation of the Spherical Harmonic Gravity Series for Numerical Orbital Propagation," *AAS/AIAA Space Flight Mechanics Meeting*, American Astronomical Soc. Paper 15-440, Washington, D.C., 2015.

[20] Macomber, B., Probe, R., Woollands, A., Read, J., and Junkins, J., "Enhancements for Modified Chebyshev–Picard Iteration Efficiency for Perturbed Orbit Propagation," *Computer Modeling in Engineering Sciences* (submitted for publication).

[21] Macomber, B., Probe, A., Woollands, R., and Junkins, J., "Automated Tuning Parameter Selection for Orbit Propagation with Modified Chebyshev–Picard Iteration," *AAS/AIAA Space Flight Mechanics Meeting*, American Astronomical Soc. Paper 15-417, Washington, D.C., 2015.

[22] Woollands, R., Bani Younes, A., and Junkins, J., "A New Solution for the General Lambert Problem," *37th Annual AAS Guidance and Control Conference*, American Astronomical Soc. Paper 14-017, Washington, D.C., 2014.

[23] Miele, A., and Iyer, R., "General Technique for Solving Nonlinear, Two-Point Boundary value Problems via the Method of Particular Solutions," *Journal of Optimization Theory and Applications*, Vol. 5, No. 5, 1970, pp. 382–399. doi:10.1007/BF00928674

[24] Woollands, R., Read, J., Macomber, B., Probe, A., Bani Younes, A., and Junkins, J., "Method of Particular Solutions and Kustaanheimo–Stiefel Regularized Picard Iteration for Solving Two-Point Boundary Value Problems," *AAS/AIAA Space Flight Mechanics Meeting*, American Astronomical Soc. Paper 15-373, Washington, D.C., 2015.

[25] Woollands, R., Bani Younes, A., Macomber, B., Bai, X., and Junkins, J., "Optimal Continuous Thrust Maneuvers for Solving 3-D Orbit Transfer Problems," *38th Annual AAS Guidance and Control Conference*, American Astronomical Soc. Paper 15-082, Washington, D.C., 2015.

[26] Koblick, D., and Shankar, P., "Evaluation of the Modified Picard-Chebyshev Method for High-Precision Orbit Propagation," *Journal of Aerospace Engineering*, Vol. 28, No. 5, Sept. 2015. doi:10.1061/(ASCE)AS.1943-5525.0000463

[27] Macomber, B., "Enhancements of Chebyshev–Picard Iteration Efficiency for Generally Perturbed Orbits and Constrained Dynamical Systems," Ph.D. Dissertation, Texas A&M Univ., College Station, TX, 2015.

[28] Engels, R., and Junkins, J., "The Gravity-Perturbed lambert Problem: A KS Variation of Parameters Approach," *Celestial Mechanics*, Vol. 24, No. 1, May 1981, pp. 3–21.

[29] Kriz, J., "A Uniform Solution of the Lambert Problem," *Celestial Mechanics*, Vol. 14, No. 4, Dec. 1976, pp. 509–513. doi:10.1007/BF01229061

[30] Kustaanheimo, P., and Stiefel, E., "Perturbation Theory of Kepler Motion Based on Spinor Regularzation," *Journal fur die Reine und Angewandt Mathematik*, Vol. 1965, No. 218, Jan. 1965, pp. 204–219.

[31] Stiefel, E., and Scheifele, G., *Linear and Regular Celestial Mechanics*, Springer–Verlag, Berlin, 1971, pp. 18–35, 271–282.

[32] Levi-Civita, T., "Sur la Regularization du Problem des Trois Corps," *Acta Mathematica*, Vol. 42, No. 1, Dec. 1920, pp. 99–144. doi:10.1007/BF02404404

[33] Rody, O., "RKN1210—A 12th/10th Order Runge-Kutta-Nyström Integrator," MATLAB CENTRAL, Sept. 2009.

[34] Koblick, D., "Gauss–Jackson Eighth-Order MultiStep Predictor-Corrector," MATLAB CENTRAL May 2012.